universität wien

MASTERARBEIT / MASTER'S THESIS

Titel der Masterarbeit / Title of the Master's Thesis

„Localisation and quantification of micro- and nanoplastic particles in colon cancer cells“

verfasst von / submitted by

Elisabeth Schögl, BSc

angestrebter akademischer Grad / in partial fulfilment of the requirements for the degree of

Magistra pharmaciae (Mag.pharm.)

Wien, 2023 / Vienna 2023

Studienkennzahl lt. Studienblatt / degree programme code as it appears on the student record sheet:	UA 066 605
Studienrichtung lt. Studienblatt / degree programme as it appears on the student record sheet:	Masterstudium Pharmazie
Betreut von / Supervisor:	Ass.-Prof. Mag. Dr. Verena Pichler

Abstract

The ubiquitous nature of plastics in our environment, as well as in our food and consumer packaged goods, results in inevitable human exposure and is therefore of particular concern. Due to ingestion of contaminated foods, the human gastrointestinal tract (GIT) is most likely the first site of exposure to micro- and nanoplastic (MNP) on a daily basis. The aim of the study is to analyse the uptake and intracellular fate of polystyrene- (PS) MNP particles with different sizes (0.235, 1.14 and 9.55 µm) in the human intestinal cell lines HT29, HCT116, SW480 and SW620.

Fluorescence microscopy was used to qualitatively evaluate the influence of particle size on cellular internalization. In addition, co-localization of PS particles within the lysosomal and endosomal compartment was analysed using confocal laser scanning microscopy (CLSM). Flow cytometry experiments were performed to quantify the cellular uptake of the particles after 1, 3, 6 and 24 hours.

No uptake into cells was observed for the 9.55 µm particles. Internalization of 1.14 and especially 0.235 µm was widespread, with particles showing co-localization in both lysosomes and endosomes. Accumulation of the 0.235 µm particles was observed, especially in lysosomes. Adhesion to the nuclear membrane as well as uptake into the nucleus, could be demonstrated for 0.235 µm PS particles. The highest uptake rates (50.5 and 89.5%) after 24 hours were determined for HCT116 cells for both PS 1.14 and 0.25 µm particles, respectively. Both PS particles sizes were found to accumulate in all four colon cancer cell lines in a dose-dependent manner. At low concentrations (0.1 µg/ml), 1.14 µm PS particles showed almost no interactions with the two cell lines HT29 (3.5%) and SW620 (5.8%). For HCT116 (12.3%) and SW480 (11.6%) cells, slightly higher interaction rates were observed. The general tendency for particle-cell interactions was by far higher for 0.235 µm particles. Even at low concentrations of 0.1 µg/ml, uptake rates of up to 41.7% (for HCT116) were observed.

The present results suggest that human intestine cells, internalize PS-MNP particles and that the size of the particles and the cell type plays an important role in the uptake process and the intracellular distribution.

Zusammenfassung

Da Kunststoffe in unserer Umwelt sowie in unseren Lebensmitteln und verpackten Konsumgütern allgegenwärtig sind, führt dies zu einer unvermeidlichen Exposition des Menschen. Aufgrund der Aufnahme kontaminierter Lebensmittel ist der menschliche Magen-Darm-Trakt (GIT) höchstwahrscheinlich der erste Ort der täglich Mikro- und Nanoplastik (MNP) ausgesetzt ist. Ziel der Arbeit ist die Untersuchung der Aufnahme und des intrazellulären Verbleibs von Polystyrol (PS) MNP-Partikeln unterschiedlicher Größe (0,235, 1,14 und 9,55 µm) in den humanen Darmkrebszelllinien HT29, HCT116, SW480 und SW620.

Fluoreszenzmikroskopie wurde zur qualitativen Bewertung des Einflusses der Partikelgröße auf die zelluläre Internalisierung eingesetzt. Eine Lokalisierung der PS Partikeln innerhalb des lysosomalen und endosomalen Kompartiments erfolgte mittels konfokaler Laser-Scanning-Mikroskopie. Durchflusszytometrie-Experimente wurden durchgeführt, um die zelluläre Aufnahme der Partikel nach 1, 3, 6 und 24 Stunden zu quantifizieren.

Für die 9,55 µm Partikel wurde keine Aufnahme in die Zellen beobachtet, jedoch konnte eine Internalisierung der 1,14 und 0,235 µm Partikeln nachgewiesen werden, welche sowohl in den Lysosomen als auch in den Endosomen lokalisiert wurden. Eine Anhäufung der 0,235 µm Partikel wurde vor allem in den Lysosomen beobachtet. Die Adhäsion an der Kernmembran sowie die Aufnahme in den Zellkern konnte für die 0,235 µm PS Partikel nachgewiesen werden. Die höchsten Aufnahmeraten (50,5 und 89,5%) nach 24 Stunden wurden bei HCT116-Zellen für die PS 1,14 bzw. 0,235 µm Partikel bestimmt. Beide PS Partikelgrößen reicherten sich dosisabhängig in allen vier Darmkrebszelllinien an. Bei niedrigen Konzentrationen (0,1 µg/ml) zeigte sich nur eine äußert geringe Aufnahme der 1,14 µm PS Partikel in die beiden Zelllinien HT29 (3,5%) und SW620 (5,8%). Bei den Zellen HCT116 (12,3 %) und SW480 (11,6 %) wurden geringfügig höhere Internalisierungsraten beobachtet. Die allgemeine Tendenz für Partikel-Zell-Interaktionen war bei 0,235 µm Partikeln deutlich höher. Selbst bei niedrigen Konzentrationen von 0,1 µg/ml wurden Aufnahmeraten von bis zu 41,7 % (für HCT116) beobachtet.

Die vorliegenden Ergebnisse legen nahe, dass menschliche Darmzellen in der Lage sind, PS-MNP-Partikel zu internalisieren und dass die Größe eine wichtige Rolle bei der Aufnahme und der intrazellulären Verteilung spielt.

TABLE OF CONTENTS

List of figures

List of tables

List of abbreviations

ABC	ATP-binding cassette
ARF6	ADP-ribosylation factor 6
BMDC	Bone marrow-derived dendritic cells
BPA	Bisphenol-A
BSA	Bovine Serum Albumin
CCV	Clathrin coated vesicle
CDC42	Cell division cycle 42
CLSM	Confocal laser scanning microscopy
CME	Clathrin - mediated endocytosis
CMS	Consensus molecular subtype
CR-3	Complement receptor type 3
CvME	Caveolin - mediated endocytosis
EFSA	European Food Safety Authority
EMT	Epithelial mesenchymal transition
EPS	Polystyrene – expandable
FBS	Fetal Bovine Serum
Fc-gamma R	Fragments crystallisable gamma receptor
FSC	Forward scattered light
GIT	Gastrointestinal tract
Hsc70	Heat shock cognate protein 70
IL-10	Interleukin-10
IL-8	Interleukin-8
IMM	Ibidi Mounting Medium
MEM	Minimum Essential Medium
MNP	Micro- and nanoplastic
MP	Microplastic
NP	Nanoplastic
P/S	Penicillin-Streptomycin
PAH	Polycyclic aromatic hydrocarbons
PBDE	Polybrominated diphenyl ether
PBS	Phosphate Buffered Saline

PCB	Polychlorinated biphenyls
PE	Polyethylene
PE-HD	Polyethylene – high density
PE-LD	Polyethylene – low density
PE-LLD	Polyethylene – linear low density
PE-MD	Polyethylene – medium density
PET	Polyethylene terephthalate
PFA	Paraformaldehyde
PMT	Photomultiplier tubes
POP	Persistent organic pollutants
PP	Polypropylene
PS	Polystyrene
PUR	Polyurethane
PVC	Polyvinyl-chloride
RhoA	Ras homolog family member A
ROS	Reactive oxygen species
SSC	Side scattered light
SSC-A	Side scatter area
SSC-H	Side scatter height
TGFβ	Transforming growth factor β
UV	Ultraviolet

1. Introduction

1.1 Evolution of plastic

Since the synthesis of the first fully synthetic plastic back in 1909, plastic materials have played an important role in daily live (Hesler et al., 2019). Not only are they applied for safety and comfort to the society (PlasticsEurope, 2019), plastics also have played a significant role in revolutionizing healthcare. Gloves, disposable syringes, blood bags, heart valves, prostheses and more are some of the many ways plastics can be used to create medical devices ("Healthcare - Plastics Europe," n.d.). Still the largest end-use market remains the packaging sector (e.g. container, plastic bags, food packaging for dairy or fishery) with around 44% of the global demand, followed by building and construction (i.e. building insulation) (18%), the automotive sector (i.e. lightweight vehicle) (8%), electrical & electronics (7%), household, leisure and sports (7%), agriculture, farming and gardening (4%) and others (12%) (PlasticsEurope, 2022).

Due to their versatility, low production costs and low weight, usage of plastics has increased steadily (Rubio et al., 2020). Back in the 1950s, when the industrial production of plastic started, about 1.5 million tons were produced (Hesler et al., 2019). Since then the amount has raised to 245 million tons in 2008 (Lithner et al., 2011) and from the years 2020 to 2021 from 375.5 to 390.7 million tons worldwide. Major producer is China (32%) followed by North America (Canada, Mexico, United States) (18%), the rest of Asia (17%) and Europe (15%). In 2021, 57.2 million tonnes of plastic were produced in Europe, while only 29.5 million tonnes of plastic waste ended up in the waste stream management. The world-wide plastic recovery is even lower (PlasticsEurope, 2022). Worldwide about 1.4 billion tons of waste are generated per year, thereof plastic made up at least 10% (Chang et al., 2020). It is estimated that more than 8-10 million tons of plastic waste end up in the ocean each year (Banerjee and Shelver, 2021; Rudolph et al., 2021), whether due to a lack of recycling capacity, illegal dumping or littering (Hesler et al., 2019). That in turn causes about 250.000 tons of plastic pieces to float on the surface in the oceans (Banerjee and Shelver, 2021) as so-called "garbage patches" (Hesler et al., 2019). Not only the oceans, but also the terrestrial environment is affected by plastic pollution. It is assumed that the contamination on land is 4-23 fold higher (Rudolph et al., 2021).

1.2 Definition and classification of plastic

The word “plastic” or “plastics” comes from the Greek word “plastikos”, meaning “to form” or that something is capable of being molded. Today plastics are defined not only as one material, they represent a broad group of diverse materials with different properties and applications. They are durable, versatile, easy to form, lightweight, robust, highly adaptable (PlasticsEurope, 2018), ductile, corrosion resistant, thermal and electrical insulating and much more (Andrady and Neal, 2009).

Plastics are synthetic or semi-synthetic organic materials, (Chang et al., 2020) that can be produced from different feedstocks. Usually, most plastic materials are fossil-based, made out of gas or oil, but they can also be produced from renewable resources, e.g. sugar, starch, vegetable oils (castor -, soy - beans or rapeseed) etc., or from mineral-based sources (salt) (Lithner et al., 2011; PlasticsEurope, 2019).

Plastic can be categorized into two types: Thermoplastics and Thermosets (Figure 1). Both are polymers, but react differently when exposed to heat. Thermoplastics are linear polymers that soften when heated and can be remolded multiple times. The molecules of these polymers are synthesized as long linear fibres and do not undergo a chemical change in the molding operation. Examples contain PE (polyethylene), PP, (polypropylene), PVC (polyvinyl-chloride), PET (polyethylene terephthalate), PS (polystyrene) and more (Figure 2). Thermosets are cross-linked polymers, which remain solid and keep their form under heat once they are cured, due to an irreversible chemical reaction when heated. Unlike thermoplastics, thermosets cannot be remelted, reshaped or recycled as a result of the polymerisation process. Thermosets comprise PUR (polyurethane), unsaturated polyesters, phenol-formaldehyde resins, silicone, etc. (Patel et al., 2022; PlasticsEurope, 2019).

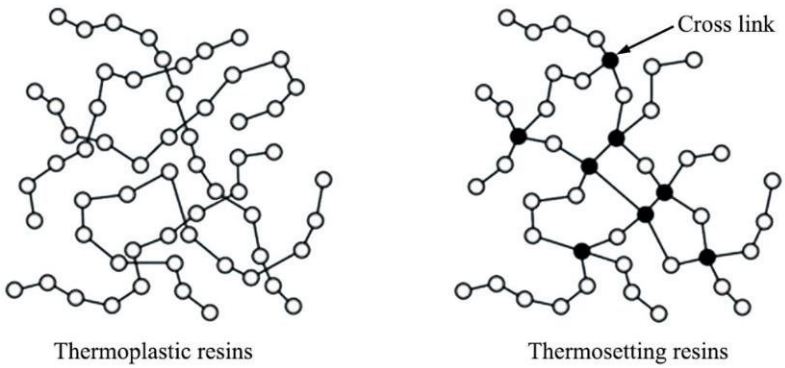

Figure 1. Molecular structure of thermoplastics and thermosets (Karuppiah, 2016)

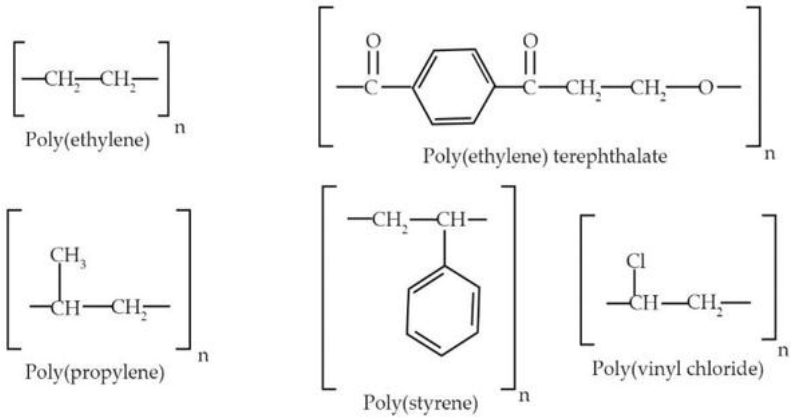

Figure 2. Molecular structures of major commercial thermoplastic polymers (Glaser, 2019)

In total there are more than 20 different types of polymers. The major types are PE, PP, PVC, PS, PET and PUR, also known as the "big six" (PlasticsEurope, 2012) regarding to their high market share of ~76% worldwide (PlasticsEurope, 2022). The typical applications sectors of these polymers are given in Table 1.

Table 1. Plastic demand distribution by polymer types. (PlasticsEurope, 2019)

Resin types	Plastic demand
PE-LD, -LLD	Reusable bags, trays and containers, agricultural film, food packaging film, etc.
PE-HD, -MD	Toys, milk bottles, shampoo bottles, pipes, houseware, etc.
PP	Food packaging, sweet and snack wrappers, hinged caps, microwave containers, pipes, automotive parts, bank notes, etc.
PVC	Window frames, profiles, floor and wall covering, pipes, cable insulation, garden hoses, inflatable pools, etc.
PS, EPS	Food packaging, building insulation, electrical and electronic equipment, inner liner for fridges, eyeglasses frames, etc.
PET	Bottles for water, soft drinks, juices, cleaners, etc.
PUR	Building insulation, pillows and mattresses, insulating foams for fridges, etc.

In commercial plastics, polymers are usually mixed with other substances called additives, e. g. to facilitate processing and to give them certain properties that are important for the final product (Lithner et al., 2011). These include antioxidants, UV (ultraviolet), e.g. bisphenol-A (BPA), and thermal stabilizer, flame retardants, plasticizers (e.g. phthalates),

curing agents, fillers and reinforcements to enhance the performance as well as various additives to improve the appearance, e.g. colorants, organic and inorganic pigments, flatting and opacifying agents (Andrady and Neal, 2009; Sendra et al., 2021). Additives can make up to 70% of the total weight of plastics, e.g. plasticizer and fire retardants can amount 10 - 70% and fillers up to 50% (Sendra et al., 2021).

1.3 Micro – and nanoplastics

Microplastics (MPs) are defined as particles with a size between 0.1 µm and 5 mm. Plastic particles less than 100 nm in diameter are considered nanoplastics (NPs) (Liu et al., 2021).

1.3.1 Sources and formation

MNP particles can be classified into two categories, primary and secondary plastic particles. Primary MNP particles are intentionally produced at the micro- or nanoscale and are widely used in paints (Rubio et al., 2020), soaps, scrubs, facial cleansers, toothpastes, in the biomedical fields (Hwang et al., 2020) as drug carriers or even in the industry for air blasting technologies (Banerjee and Shelver, 2021). In contrast to primary microplastic particles, secondary microplastic particles are formed by fragmentation of plastic litter (Jiang et al., 2020). As soon as plastic waste enters the environment, it can be slowly degraded by photo- and thermo-oxidative processes, mechanical abrasion and, to a small extent, by biodegradation (Visalli et al., 2021). Factors such as UV radiation, wind, waves and other influences weaken the material integrity and cause the plastic to become brittle and fragmented into smaller pieces (Jiang et al., 2020). These processes can lead to molecular weight decrease (e.g. through chain scission), crosslinking or to cyclisation (Lithner et al., 2011). The micro- and nanoparticles resulting from the degradation processes are heterogeneous and differ in size, shape (ranging from fibres, cones and sticks to amorphous or irregular shapes), density, crystallinity and chemical composition (Rubio et al., 2020). Furthermore, during the aging process of the plastic, mainly due to photodegradation, a modification of the structural composition of the polymer may occur, resulting in the formation of oxygen-containing functional groups on the surface of the particles (Liu et al., 2019; Rowenczyk et al., 2020). However, such surface alterations may facilitate the uptake of environmental pollutants such as metals or persistent organic pollutants (POPs) (Visalli et al., 2021).

1.3.2 Occurrence in the environment and routes of exposure

MP and NP are present in both aquatic and terrestrial ecosystems. They are found in oceans, freshwater, sediments, soil, air, food (Jiang et al., 2020; Prata et al., 2020) and even in the sea ice of the Arctic (Hesler et al., 2019).

Plastic can pose a threat to marine species, not only through entanglement (e.g. nets, ropes, fishing lines, plastic bags etc), but also through the ingestion of MP and NP (Wilcox et al., 2016). MP and NP particles have been detected in numerous aquatic organisms, starting at the lowest level, such as zooplankton, up to invertebrates (e. g. crustacea) and vertebrates (e.g. fish) (Chang et al., 2020; EFSA Panel on Contaminants in the Food Chain (CONTAM), 2016; Rubio et al., 2020). Plastic particles that are ingested by these marine organisms can accumulate in their bodies and subsequently reach humans via the food chain. One of the most worrisome food sources for humans are bivalves, such as mussels, oysters, shellfish etc. In aquatic organisms, the largest amounts of MPs and NPs are found in their digestive tract. Compared to fish, the digestive tract of bivalves is not removed before consumption. For example, according to the European Food Safety Authority (EFSA), the intake of 225 g mussels can lead to an exposure of up to 7 µg of plastic (EFSA Panel on Contaminants in the Food Chain (CONTAM), 2016; Jiang et al., 2020).

Ingestion of contaminated seafood is one way humans can come into direct contact with plastic particles. MP and NP particles have also been detected in other food products, including beer, salt, honey, sugar, tap and bottled water (Hesler et al., 2019; Prata et al., 2020; Rubio et al., 2020; Sendra et al., 2021; Visalli et al., 2021), as well as in food packaging, e.g. tea bags and coffee capsules (Banerjee and Shelver, 2021; Visalli et al., 2021). The estimated annual consumption of microplastics through food intake is 39,000-52,000 particles per person. This value increases to 74,000-121,000 when inhalation of these particles is included. In addition, up to 90,000 MP particles can be ingested annually if the water intake only occur through bottled sources, compared to additional 4,000 MP particles if only tap water is consumed (Cox et al., 2019). The presence of microplastics in human faeces has been confirmed in recent studies so far and suggests that humans are exposed to microplastics via food and/or beverages (Schwabl et al., 2019; Zhang et al., 2021).

In principle ingestion is considered to be the major route of MP and NP exposure to humans (Visalli et al., 2021) (Figure 3). However, these plastic particles can also be transported into the air, e.g. by detachment of fibres from clothing made of synthetic textiles or by abrasion of car tires, and thus inhaled (Hesler et al., 2019; Prata et al., 2020; Rubio et al., 2020).

Dermal exposure is considered less important. While it may be possible for nanoparticles (<100 nm) to cross the skin barrier, this route appears less likely. Rather, the dermal pathway is correlated with the exposure to plastic additives, e.g. BPA or phthalates (Prata et al., 2020; Revel et al., 2018; Rubio et al., 2020).

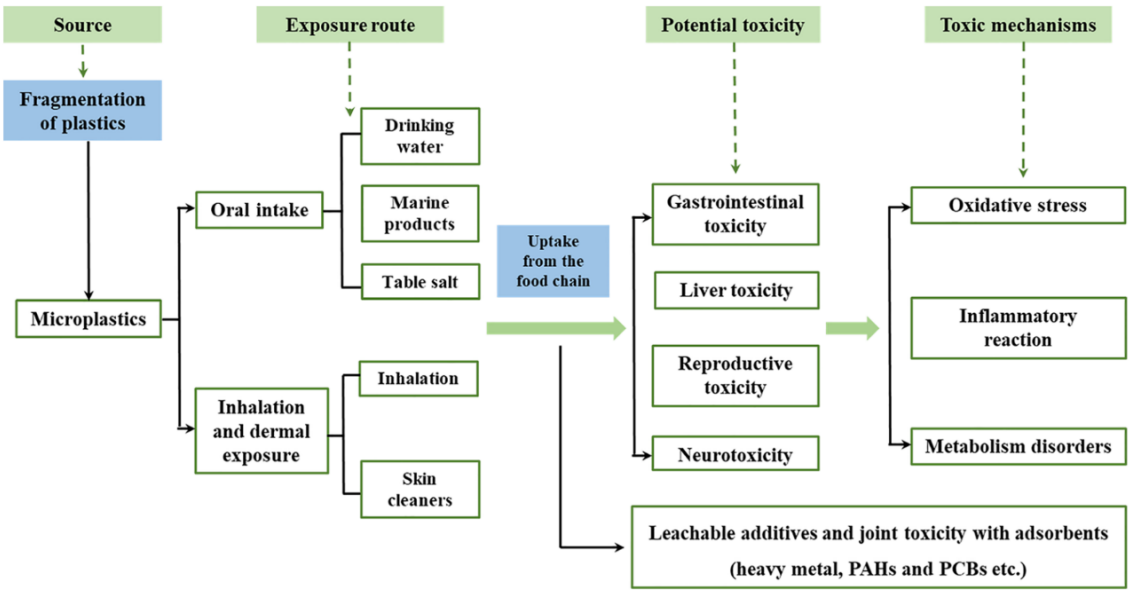

Figure 3. Overview of the potential routes of exposure and toxicity pathways (Chang et al., 2020)

1.4 Pathways of micro - and nanoplastic toxicity

Plastic polymers have been considered inert and non-hazardous to human health for a long period of time, but recent studies indicate that direct contact with MP and NP particles can potentially lead to adverse effects at cellular levels (Hwang et al., 2020; Revel et al., 2018) (Figure 3). To date, there have been numerous studies on the presence of MP/NPs and their possible effects on marine organisms, but information on their potential toxic effects in humans is scarce (Chang et al., 2020).

Lithner et al. developed a hazard classification model for plastic polymers based on the hazard category of the respective monomers. Of the 55 polymers studied, polyurethanes, polyacrylonitriles, polyvinyl chloride, epoxy resins and styrene-based polymers were found to be the most hazardous in terms of the mutagenic and carcinogenic classification (category 1A/1B) of the monomers (Lithner et al., 2011). Thus, the toxicity of MP and NP particles appears to be due to 3 different factors - the nature of the polymers itself (i.e. polymer type), the leaching of additives and the adhesion of pollutants (Rubio et al., 2020).

1.4.1 Toxicity in vivo

Apart from the type of the polymer, there are several factors that influence toxicity, such as the size of the particles. According to EFSA, particles larger than 150 µm in diameter are not able to invade the mucosal barrier and should therefore only lead to local effects in the intestine. Though, particles smaller than 150 µm in diameter could pass through the intestinal mucosal barrier, potentially leading to systemic exposure. However, it is assumed that the absorption of these particles is extremely low (< 0.3%). Only particles smaller than 1.5 µm in diameter are expected to penetrate deeper tissues/organs. (EFSA Panel on Contaminants in the Food Chain (CONTAM), 2016).

The effects of micro- and nanoplastic particles on the intestinal epithelium have been investigated in numerous *in vivo* studies, demonstrating an intestinal effect in invertebrates (e.g. nematodes, mussels) and vertebrates (e.g. zebrafish) as well as in mammals (e.g. mice) (Hirt and Body-Malapel, 2020). Pathological changes of the intestine include a decrease in mucus secretion, gut barrier dysfunction, intestinal inflammation and dysbiosis of the intestinal microbiota (Visalli et al., 2021; Yong et al., 2020).

Especially the diversity of the gut microbiome plays an important role in human health. Several studies have shown that MP and NP can alter the diversity and composition of the gut microbiome (Huang et al., 2021), which can subsequently disrupt physiological homeostasis and may lead to various diseases such as cardiovascular or neurological diseases, inflammation and cancer (Kannan and Vimalkumar, 2021). However, such a dysbiosis is also related to diabetes (Huang et al., 2021), inflammatory bowel diseases (Li et al., 2020) or even obesity (Kannan and Vimalkumar, 2021). Furthermore, a change in the composition of the gut microbiome may affect immune function. Certain bacteria, such as *Firmicutes* and *Bifidobacterium*, can induce the differentiation of Treg cells (regulatory T cells) and modulate inflammatory processes by promoting the secretion of pro- and anti-inflammatory cytokines (e.g. IL-10 or IL-8) (Li et al., 2020).

Research has shown that exposure to MP particles may also lead to disorders in energy metabolism, as well as bile acid (Kannan and Vimalkumar, 2021; Yong et al., 2020) and amino acid metabolism. Whereas both, bile acids and amino acids, are in turn linked to the intestinal microbiota (Jin et al., 2019).

1.4.2 Toxicity in vitro

Numerous studies have investigated the effects of MP and NP particles on human cell cultures. Although cellular uptake was observed to some extent, there was generally little or no evidence of cellular toxicity in most *in vitro* studies, except at very high concentrations. The two most commonly documented effects are the production of reactive oxygen species (ROS) and inflammatory responses (Visalli et al., 2021; Yong et al., 2020).

Small plastic particles can interact with the cell membrane and then be internalized. The generated ROS lead to oxidative stress and this can subsequently cause cytotoxicity and DNA damage (Visalli et al., 2021), e.g. double strand breaks or point mutations of the DNA (Fröhlich, 2012). If these mutations regulate key genes that are involved in cell cycle control for example, this could subsequently trigger carcinogenesis (Rubio et al., 2020). Moreover, some plastic particles are associated with a disruption of the mitochondrial membrane potential and in turn also with the inhibition of the activity of the toxin efflux pump, ATP-binding cassette (ABC) transporter, leading to increased arsenic exposure (Visalli et al., 2021; Wu et al., 2019).

1.4.3 Plastic additives and contaminants

MP and NP particles contain a number of additives (4% w/w on average) and can also adsorb chemical pollutants (both organic or inorganic substances) (EFSA Panel on Contaminants in the Food Chain (CONTAM), 2016; Hirt and Body-Malapel, 2020). Both, additives and chemical contaminants, can have a variety of toxic effects, including carcinogenic and mutagenic effects (Lithner et al., 2011).

The main additives of concern for human health are phthalates, bisphenols, brominated flame retardants and organotins, which can leach from the surface of MP and NP particles (Paul et al., n.d.). BPA, phthalates and brominated flame retardants can act as endocrine disruptors by interfering with a number of hormones even at very low doses (Prata et al., 2020) and are further linked to chronic diseases such as diabetes, obesity, metabolic disorders or even cancer. Brominated flame retardants, e.g. polybrominated diphenyl ethers (PBDEs) can also impair fertility, as they affect hormone levels of oestrogens and thyroid hormones in particular (Sendra et al., 2021). Furthermore, metal - based catalyst e.g. antimony (Sb), who are used for the production of PET water bottles, can be released into the water at high temperatures (above 60 °C) (Banerjee and Shelver, 2021; Revel et al.,

2018). In addition to additives, MP and NP particles can also release carcinogenic monomers, such as propylene oxide or acrylonitrile (Lithner et al., 2011).

Due to their high surface to volume ratio and hydrophobicity, MP and NP particles can adsorb other contaminants and thus act as a so called "Trojan horse". Therefore they can serve as carriers for POPs, such as polycyclic aromatic hydrocarbons (PAHs), polychlorinated biphenyls (PCBs) (Banerjee and Shelver, 2021; Prata et al., 2020; Rubio et al., 2020) and organochlorine pesticides (Landrigan et al., n.d.) or for heavy metals (e.g. cadmium, chromium, aluminium, zinc, cobalt, etc.) (Banerjee and Shelver, 2021). The uptake of MP and NP particles therefore raises concerns that organisms are exposed to higher concentrations of potentially toxic substances (Prata et al., 2020).

Furthermore, plastic particles can contain numerous microorganisms that form biofilms on their surface. Thus, MP and NP particles can also serve as vectors for microorganisms such as pathogenic Vibrio spp. or E. coli (Hirt and Body-Malapel, 2020; Prata et al., 2020).

1.5 Cellular uptake mechanisms of micro - and nanoplastics

The epithelium of the gut represents an important barrier-exchange system (Inkielewicz-Stepniak et al., 2018). It is composed of several cell types including enterocytes (mainly responsible for the absorption of nutrients), goblet cells (secrete mucus), enteroendocrine cells (produce hormones), microfold cells (transport antigens) and others (Huang et al., 2021; Stock et al., 2019). To maintain the integrity of the epithelium, epithelial cells are connected to each other through an intercellular junction complex composed of tight junctions, adherens junctions and gap junctions. Particular importance is given to tight junctions, which play an important role in the regulation of the endothelial barrier function (Huang et al., 2021; Mehta and Malik, 2006). Tight junctions prevent the passage of larger molecules and unwanted substances and maintain the differences between apical and basolateral sides, ensuring the polarity of the cell (Burkey et al., 2009; Gullberg, 2005). By sealing the intercellular spaces, paracellular transport is regulated (Schneeberger and Lynch, 2004).

There are two routes the epithelium can be permeated: transcellular (path through the cells) or paracellular (path between the cells) (Daugherty and Mrsny, 1999; Fröhlich and Roblegg, 2012) (Figure 4). However, the paracellular route seems improbable for MNPs, considering the particle size and the maximum pore radii (~ 1.5 nm) of the tight junctions, the transcellular uptake by passive penetration may be possible, albeit limited. The most likely

route for MNP particle uptake appears to be endocytosis (Banerjee and Shelver, 2021; EFSA Panel on Contaminants in the Food Chain (CONTAM), 2016; Fröhlich and Roblegg, 2012).

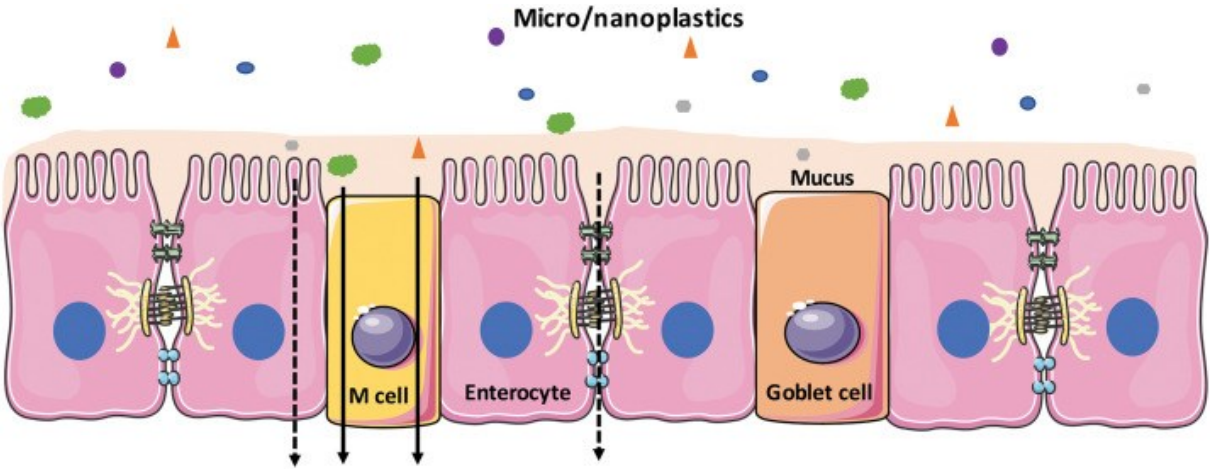

Figure 4. Schematic view of the transport mechanisms of micro- and nanoplastics through the intestinal epithelium (Banerjee and Shelver, 2021)

The internalization of MNP particles is influenced by several factors, such as size, shape, surface charge and surface chemistry of the particles as well as the cell type itself (Liu et al., 2021; Shang et al., 2014). The uptake of particles > 500 nm is considered to occur via phagocytosis, particles < 500 nm are take up into the cell via other endocytotic mechanisms (Kumari et al., 2010). The term endocytosis encompasses various mechanisms that enable the cell to internalise molecules and macromolecules. These are transported into the cell in membrane-bound vesicles, which are formed by the invagination and the pinching-off of parts of the plasma membrane (Canton and Battaglia, 2012). The main different mechanisms of endocytosis are phagocytosis, macropinocytosis, clathrin – mediated endocytosis, caveolin – mediated endocytosis and the clathrin – and caveolin independent pathways (Figure 5).

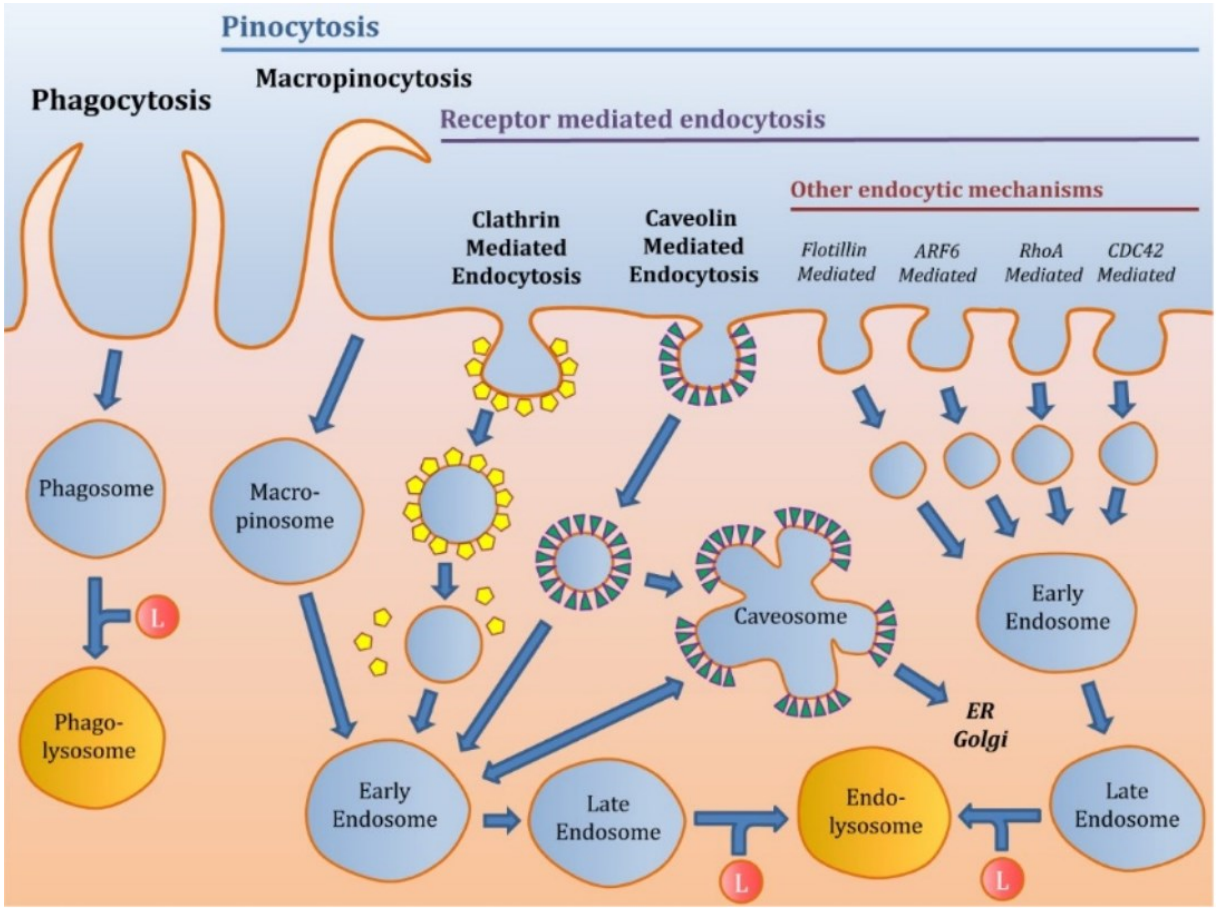

Figure 5. Overview of uptake mechanisms into cells (Manzanares and Ceña, 2020)

1.5.1 Phagocytosis

Phagocytosis is an essential process for the uptake of pathogenic microorganisms, cell debris, dead cells and exogenous material. This is generally performed by professional phagocytes, such as dendritic cells, monocytes/macrophages and neutrophils, although other cells such as epithelial and endothelial cells are also capable of phagocytosis in rare situations. Phagocytosis is usually initiated by opsonization, i.e. adsorption of immunoglobulins, complement proteins or other serum proteins on the particle surface. Thus, opsonized particles can be detected and subsequently bound by the activation of surface receptors of the phagocytes (Behzadi et al., 2017; Canton and Battaglia, 2012; Donahue et al., 2019), e.g. the Fc-gamma R (fragment crystallisable gamma receptor), the CR-3 (complement receptor type 3) and others (Canton and Battaglia, 2012; Kumari et al., 2010). This leads to the formation of membrane invaginations that engulf the particle. A so-called phagosome is formed that can fuse with a lysosome to form a phagolysosome, which can digest foreign material and render it harmless (Donahue et al., 2019; Kumari et al., 2010).

1.5.2 Macropinocytosis

Macropinocytosis is a non-specific mechanism whereby larger amounts of fluid can be taken up into the cell. In this actin-driven process, the cytoskeleton is restructured, forming large membrane extensions that subsequently fuse with the membrane again. Thereby, particles and other components are taken up together with the extracellular fluid into large vesicles (> 0.2 µm), so-called macropinosomes (Behzadi et al., 2017; Canton and Battaglia, 2012; Donahue et al., 2019).

1.5.3 Clathrin – mediated endocytosis

Clathrin - mediated endocytosis (CME) is one of the most important mechanism of cells to obtain nutrients. CME is a multistep process and begins with the re-sorting/clustering of transmembrane receptors after the binding of their ligands (Behzadi et al., 2017; Canton and Battaglia, 2012; Rennick et al., 2021). This leads to the recruitment of cytosolic adaptor and accessory proteins that are responsible for the nucleation of clathrin. This nucleation facilitates the assembly of clathrin triskelions into a curved polygonal lattice, which stabilizes the deformation of the anchored membrane. The invagination of the membrane then leads to the formation of a clathrin – coated vesicle (CCV) with a size of around 100 – 150 nm in diameter. Such CCVs are then pinched off the plasma membrane by dynamin, a large GTPase that wraps around the neck of the vesicle, releasing it into the cytosol (Behzadi et al., 2017; Canton and Battaglia, 2012; Doherty and McMahon, 2009). The clathrin basket is then detached from the vesicle by auxilin and hsc70 (heat shock cognate protein 70) (Doherty and McMahon, 2009). The content of the vesicle is then delivered to an early endosome, which develop into a late endosome and eventually fuse with a lysosome (Manzanares and Ceña, 2020).

1.5.4 Caveolin – mediated endocytosis

The caveolin – mediated endocytosis (CvME) is important for a variety of functions, such as cell signalling, transcytosis, and regulation of lipids, fatty acids and membrane proteins. Caveolae are flask-shaped invaginations of the plasma membrane with a size of about 50 – 80 nm (Behzadi et al., 2017; Canton and Battaglia, 2012). They are special lipid rafts (Manzanares and Ceña, 2020) whose main component, the protein caveolin, is integrated into the membrane. So far, three different caveolin proteins are known: Caveolin – 3, which

occurs in muscle cells, and Caveolin – 1 and – 2 in non-muscle cells. Caveolin – 1 polymerizes and binds cholesterol and fatty acids, resulting in invagination and formation of caveolae. However, the exact function of Caveolin – 2 is not yet known (Canton and Battaglia, 2012; Doherty and McMahon, 2009). The formed caveolin vesicles can fuse with each other to build a so-called caveosome. This multicaveolar structure can either fuse with an early endosome or be transferred to the Golgi apparatus and the endoplasmic reticulum (Donahue et al., 2019; Manzanares and Ceña, 2020).

1.5.5 Other pathways

In addition to the previously described mechanisms, there are other pathways that can be summarized under the term clathrin- and caveolin-independent endocytosis.
These include the RhoA- (Ras homolog family member A), CDC42- (cell division cycle 42), ARF6- (ADP-ribosylation factor 6) and the flotillin- dependent pathway. However, these processes are not discussed further as they do not contribute significantly to the uptake of MNPs (Canton and Battaglia, 2012; Manzanares and Ceña, 2020).

2. Objectives

Since ingestion is considered to be the main route of potential human exposure to MNP particles, the contamination of food with these particles is of particular concern. To date, several *in vivo* studies have shown pathological changes in the intestine due to ingestion of these particles, including a decrease in mucus secretion, inflammation, dysbiosis of the intestinal microbiota and so on. However, knowledge regarding the uptake and fate of MNP particles, especially at cellular level, is limited.

Hence, the aim of this work is to examine the interaction between different PS-MNP particles and 4 different colon cancer cell lines, including

- the investigation of the influence of particle size on cellular internalization,
- the localization of MNP particles in cellular compartments, specifically the lysosomes and endosomes,
- the quantification of cellular uptake and
- the examination of the influence of cancer aggressiveness on particle uptake.

In this regard, the uptake of monodisperse spherical polystyrene-based particles with 3 different sizes (0.235, 1.14 and 9.55 µm in diameter) into 4 different human colon cancer cell lines (HT29, HCT116, SW480 and SW620) was investigated. These four cell lines were chosen to represent a model of cancer progression. Since HT29, SW480 and SW620 cells were all derived from human colon adenocarcinomas and HCT116 cells from a human colon carcinoma, it became a challenge for this work, not only to differentiate between different stages of the same disease, but also between different cancer types from the same tissue.

3. Materials and methods

3.1 Reagents and solutions

The chemicals and the solutions used in this work are specified in Table 2.

Table 2. Reagents and solutions

Description	Source of supply
Minimum Essential Medium (MEM)	Gibco®, Thermo Fischer Scientific Inc., Massachusetts, USA
Phosphate Buffered Saline (PBS)	Thermo Fischer Scientific Inc., Massachusetts, USA
Fetal Bovine Serum (FBS)	Thermo Fischer Scientific Inc., Massachusetts, USA
Penicillin-Streptomycin (P/S)	Thermo Fischer Scientific Inc., Massachusetts, USA
TrypLE™ Express (Trypsin)	Gibco®, Thermo Fischer Scientific Inc., Massachusetts, USA
0.1% Triton-X-100	Sigma – Aldrich Handels GmbH, Vienna, Austria
Paraformaldehyde (PFA)	Carl Roth GmbH + Co. KG, Karlsruhe, Germany
Bovine Serum Albumin (BSA)	Sigma – Aldrich Handels GmbH, Vienna, Austria
Trypan Blue Stain (0.4%)	Invitrogen™, Thermo Fischer Scientific Inc., Massachusetts, USA
Ibidi Mounting Medium (IMM)	Ibidi®, Ibidi GmbH, Gräfelfing, Germany
HOECHST (33342)	Invitrogen™, Thermo Fischer Scientific Inc., Massachusetts, USA
LysoTracker® Deep Red (L12492)	Invitrogen™, Thermo Fischer Scientific Inc., Massachusetts, USA
EEA1 Antibody #2411	Cell Signaling Technology, Massachusetts, USA
Goat anti-Rabbit IgG (H+L) Cross-Adsorbed Secondary Antibody, Alexa Fluor™ 633 (A-21070)	Invitrogen™, Thermo Fischer Scientific Inc., Massachusetts, USA

3.2 Equipment

Table 3 shows the equipment utilized in this work.

Table 3. Equipment

Description	Source of supply
CO_2 - Incubator Heraeus BBD 6620	Fischer Scientific GmbH, Vienna, Austria
Centrifuge Allegra X-12R	Beckman Coulter GmbH, Vienna, Austria
Centrifuge 5804 R	Eppendorf SE, Hamburg, Germany
Confocal laser scanning microscope – Leica TCS SP8-STED	Leica Microsystems GmbH, Wetzlar, Germany
IKA® - Schüttler MTS 4	IKA®-Werke GmbH & Co. KG, Staufen, Germany
Invitrogen™ Countess™ Automated Cell Counter	Fischer Scientific GmbH, Vienna, Austria
Inverted fluorescence Microscope – Nikon Eclipse TE2000-S	Nikon GmbH, Austria
Flow cytometer - BD FACSCanto™ II	BD Biosciences, New Jersey, USA
Flow cytometer - CytoFLEX S	Beckman Coulter GmbH, Vienna, Austria
Laminar flow cabinet – Thermo Heraeus Herasafe KS12	Thermo Fischer Scientific Inc., Massachusetts, USA
Vortex shaker	VWR International, Vienna, Austria

3.3 Research particles

The particles used were monodisperse, spherical polystyrene-based particles in 3 different sizes and were purchased from Microparticles GmbH (Berlin, Germany). The 9.55 µm PS particles are coloured in blue, while the 1.14 and 0.235 µm PS particles are fluorescently labelled. The exact physico- chemical properties of the used MNP particles are given in Table 4. The surface charge of the particles was not specified by the supplier. The particle solutions showed distinct differences in their calculated particle count: 9.55 µm PS particle – 1 x 10^8 ml^{-1}; 1.14 µm PS particle – 3.1 x 10^{10} ml^{-1}; 0.235 µm PS particle – 3.5 x 10^{12} ml^{-1}. To minimize PS-MNP agglomerates, the stock solution was shaken for 15 minutes and then diluted to a concentration of 100 µg/ml. Before each experiment, the solution was shaken for 15 minutes and then further diluted to the desired concentration in the respective growth media.

Table 4. Overview of the MNP particles used in the experiments

Plastic type	Form	Diameter [µm]	Fluorescence [nm]	Matrix
Polystyrene	Spherical	9.55 ± 0.13	n.a.	Aqueous (5 % w/v)
Polystyrene	Spherical	1.14 ± 0.03	Abs/Em = 530/607	Aqueous (2.5 % w/v)
Polystyrene	Spherical	0.235 ± 0.01	Abs/Em = 502/518	Aqueous (2.5 % w/v)

3.4 Cell lines

The cell lines HT29, HCT116, SW480 and SW620 were kindly provided by T. Lange, University Medical Center Hamburg-Eppendorf, in the course of the FFG-funded project microONE.

3.4.1 HT29

HT29 cells are human colorectal adenocarcinoma cells established from a primary tumour of a 44-year-old Caucasian female in 1964. HT29 are adherent cells with an epithelial morphology that show similarities to enterocytes of the small intestine. This cell line forms a multilayer of non-polarized undifferentiated cells under standard culture conditions and produces a mucin film on their surface. (Ahmed et al., 2013; Martínez-Maqueda et al., 2015; MSKCC, n.d.).

3.4.2 HCT116

HCT116 is a human colorectal carcinoma cell line derived from a 48-year-old male. Like the HT29 cell line, these cells are adherent and have an epithelial morphology (Ahmed et al., 2013; Chisanga, D. et al., 2016; "HCT.116 Cell Line Details," n.d.).

3.4.3 SW480

SW480 cells are human colorectal adenocarcinoma cells that were first isolate from a primary tumour of a 50-year-old Caucasian man (Ahmed et al., 2013; Whetzel PL et al., 2011). SW480 cells are adherent with epithelial-like morphology, which grow in monolayers (Koblitz J. et al., 2022).

3.4.4 SW620

The SW620 cell line derived from a later metastasis in the lymph node of a 51-year-old Caucasian male, the same patient from whom the SW480 cell line was isolated. Just like the other 3 cell lines, the SW620 cells are adherent and show an epithelial morphology (Ahmed et al., 2013).

3.5 Cell culture

All four cell lines were cultured in Minimum Essential Medium (MEM) supplemented with 8% FBS (fetal bovine serum) and 1% P/S (penicillin/streptomycin). The cells were cultivated in an incubator with 5% CO_2 and 95% humidity at 37°C. Cells were passaged when they reached about 70 to 80% confluency in 25 cm^2 cell culture flasks. Passaging was performed by aspirating the culture medium, washing with 5 ml phosphate buffered saline (PBS) and trypsinization with 1 ml TrypLE Express to detach the cells from the bottom of the culture flask. During trypsinization, the culture flask was incubated at 37°C for 7 minutes (HT29) or 5-7 minutes (HCT116, SW480, SW620). To stop the process, 5 ml of cell culture medium was added, and the cell suspension was transferred to a centrifuge tube. To separate the cells from the medium, centrifugation was performed at 1200 rpm for 5 minutes. The supernatant was then aspirated, and the remaining cell pellet resuspended in 5 ml culture medium. The cell count was determined, an aliquot of the cell suspension with the corresponding cell count was taken and seeded in 5 ml of culture medium in a new T-25 cell culture flask. To maintain a physiological temperature range, all fluids used were heated to 37°C in a water bath for 20 minutes prior to use.

3.6 Microscopic examinations of MNP particle internalization

Cell imaging was used as a direct detection of particle uptake and particle localization respectively, using both an inverted fluorescence microscope (Nikon Eclipse TE2000-S) and a confocal laser scanning microscope (Leica TCS SP8-STED).
It should be noted that all methods described in the following were performed the same for all four cell lines.

3.6.4 Fluorescence microscopy

For fluorescence microscopy the cells were seeded in 24-well plates (4 x 10^4 cells per well) and incubated at 37°C. After 24 hours of cultivation in the incubator, the medium was aspirated and the cells were washed once with 1 ml/well of PBS. Then the cells were incubated with PS-MNP particles, with sizes of 9.55 µm, 1.14 µm, and 0.235 µm in diameter, at 37°C for further 24 h. The cells were exposed to five different concentrations of the respective particles: 10, 1, 0.1, 0.01 and 0.001 µg/ml. The particle suspension was then aspirated, the cells were washed three times with 1 ml/well PBS to remove any particles that were not absorbed by or adhered to the cells, and new culture medium was added. The samples were observed and photographed (bright-field and fluorescent images) using the inverted fluorescence microscope Nikon Eclipse TE2000-S equipped with a mercury lamp, a Nikon digital sight DS-Qi1MC camera, and the NIS-Elements imaging software. The objective used was Nikon 20x C Plan Fluor objective. For the red and green fluorescence the Nikon filter blocks TRITC (EX 540/26, DM 565, EM 605/56) and FITC (EM 480/15, DM 505, EM 535/40) were used. "EX", "DM" and "EM" correspond to the excitation filter, the dichroic mirror, and the emission filter, respectively.

3.6.2 Confocal laser scanning microscopy

A confocal microscope was used to further confirm the particle uptake and to differentiate between internalization and cell adhesion.

In contrast to fluorescence microscopy, in which the entire fluorescence of an object is imaged, CLSM allows a precise intracellularly localization of fluorescence-labelled particles. Thereby, the laser light is focused on a defined point at a specific depth within the sample, then the selected layer is scanned point by point. Images generated by this scanning method are referred to as optical sections. By scanning and stacking several optical sections, a three-dimensional image is created (z-stack) (Paddock, 2000).

To investigate the cellular uptake of the 1.14 µm and 0.235 µm PS particles the cells were seeded in ibidi treat 8-well µ-slides (1 x 10^5 cells/ml) and incubated at 37°C for 24 hours. After the incubation the medium was removed and the cells were washed 3 times with 250 µl/well of PBS. Then the cells were exposed to 1 µg/ml of the 1.14 µm or 0.235 µm PS particles at 37°C. The concentration of 1 µg/ml was chosen because few to no particles were

visible inside the cells in the lower range. After 24 hours of treatment with the PS particles, the medium was aspirated, and the cells were washed again 3 times with PBS.
Subsequently, cells were fixated with 200 µl/well 4% paraformaldehyde (PFA) (diluted in 1X PBS) for 10 minutes at room temperature. The fixation solution was then removed, and the cells were washed thoroughly with PBS. Thereafter, cells were permeabilized with 0.1% Triton-X-100 (diluted in 1X PBS) for 15 minutes at room temperature. At the end of the incubation period, the solution was aspirated, the cells were washed 3 times with PBS and incubated with 200 µl/well 2% bovine serum albumin (BSA) in PBS to block unspecific binding sites. Treatment of the cells with the blocking solution was performed for 1 hour at room temperature. Afterwards the blocking solution was removed and the cells were washed repeatedly with PBS.
For the staining of the endosomes, the cells were first incubated with a 1:100 dilution (200 µl/well) of a primary antibody against EEA1 (EEA1 antibody, rabbit) in 1% BSA in PBS overnight at 4°C. The primary antibody solution was aspirated, and the cells were washed 3 times with PBS. Alexa Fluor 633-conjugated goat anti-rabbit IgG (H+L) cross-adsorbed antibody (dilution 1:500) was used as secondary antibody and the nuclei were stained with Hoechst 33342 (dilution 1:1000). The cells were incubated with a dilution of the secondary antibody and Hoechst dye in 1% BSA in PBS (200 µl/well) at room temperature and protected from light. After the incubation time of one hour, the solution was aspirated, the cells were washed 3 times with PBS and covered with mounting medium. Mounting medium is used to protect the sample from damage, air drying and stain fading, thus allowing storage for days or weeks. The cells were then imaged using the TCS SP8-STED confocal microscope (40 x oil objective; lasers: 405 nm and WLL2) and z-stacks were taken with a step size of 0.3 – 0.35 µm (format: 2048x2048, pixel dwell time: 1 µs, line average: 4, pinhole: 1 AU) (software LAS X).

The procedure for the staining of lysosomes differs from that for endosomes, as the LysoTracker Deep Red cannot be applied when cells are permeabilized. The LysoTracker Deep Red is a cell-permeable and red fluorescent dye that stains acidic compartments within a cell, such as lysosomes. However, permeabilisation of the cells would destroy all membranes and thus no different pH values would be present within the cells. Figure 6 shows the differences in the sequence of the individual experimental steps for the staining of lysosomes compared to endosomes.

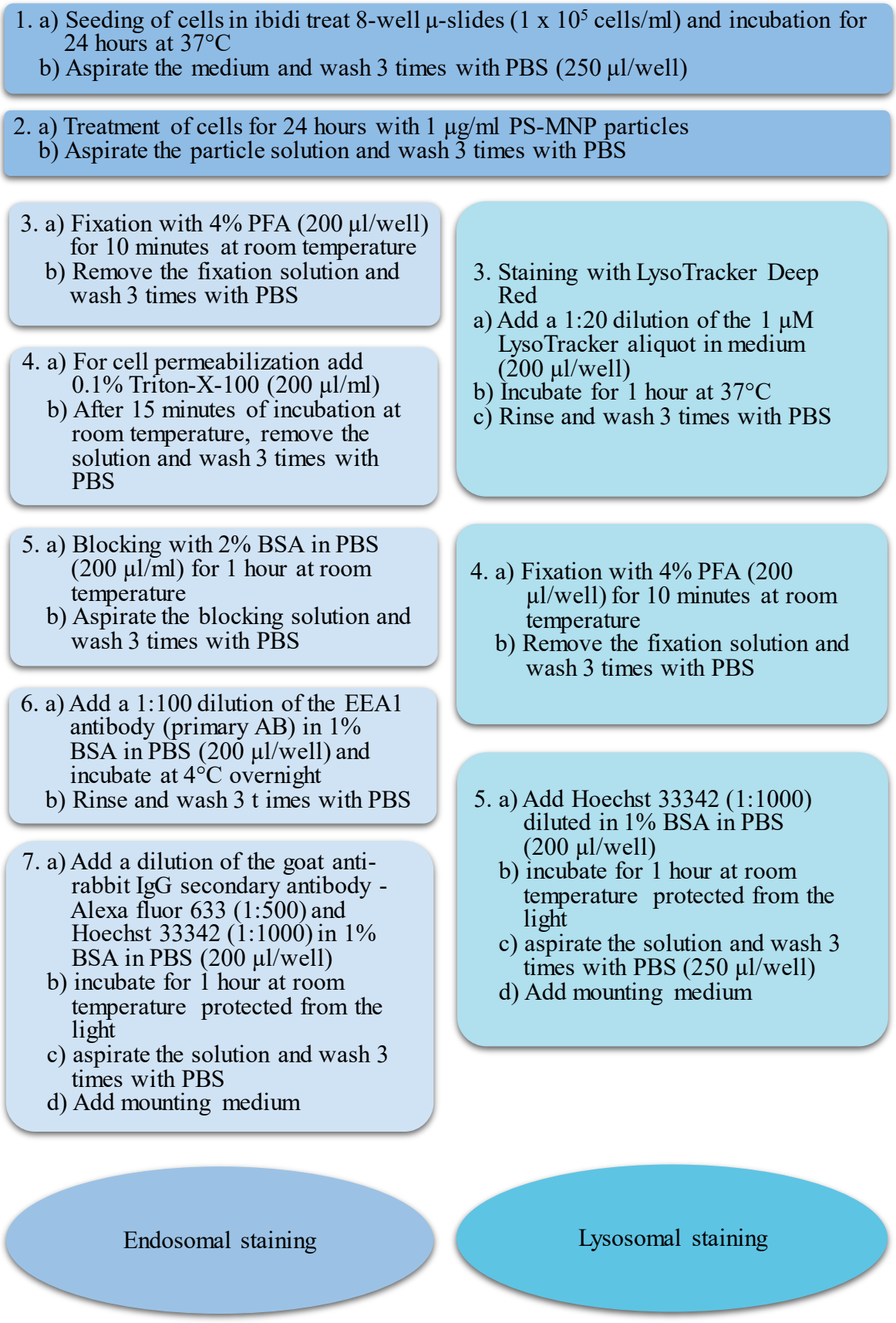

Figure 6. Implementation of an immunofluorescence staining of adherent cells

3.7 Quantification of MNP particle uptake by flow cytometry

Flow cytometry uses the principles of light scattering and fluorescence emission to measure surface and internal characteristics of single cells and particles. In the flow chamber of the flow cytometer, the sample stream is injected into the sheath fluid stream (commonly PBS) and hydrodynamically focused, creating a laminar flow and allowing the cells to pass a laser beam one at a time. The emitted light is then collected via optics and directed to detectors through a system of optical mirrors and filters that separate particular wavelengths of the light. The light signals are transformed into voltage pulses by photodetectors, e.g. photomultiplier tubes (PMTs), and digitalize for further computer analysis. Forward scattered light (FSC) is the result of diffraction and is proportional to the cell surface or size of the cells/particles. Side scattered light (SSC), on the other hand, is based on refraction and reflection and is proportional to the granularity and internal complexity of the cell. At the same time, the fluorescence of fluorescence-labelled cells or particles can be measured (Adan et al., 2017; Gompf et al., 2016).

For analysis the cells were seeded in 6-well plates at a density of 4 x 10^5/well and incubated at 37°C. After 48 hours, the medium was removed, cells were washed 1 time with 1.5 ml/well PBS and incubated with fluorescently labelled 1.14 µm and 0.235 µm PS particles. The cells were exposed to concentrations of 10, 1 and 0.1 µg/ml for 24 hours and additionally 1 µg/ml for 1, 3 and 6 hours of these particles. After the respective incubation period, the cells were washed 3 times with 1.5 ml/well PBS and detached by trypsinization with 0.5 ml/well TrypLE Express. The cells were washed and suspended in 1.5 ml/well PBS and then centrifuged (1200 rpm) for 5 minutes. After centrifugation the supernatant was discarded and the cell pellet was resuspended in 1 ml 4% PFA. After the cells were fixed for 10 minutes at room temperature, they were centrifuged again (1200 rpm, 5 minutes). The cell pellet was washed and resuspended again in PBS. After centrifugation, the solution was removed, and the cell pellet was resuspended in a FACS buffer containing 1% BSA in PBS.
Flow cytometry measurements were performed using a BD FACSCanto II and a CytoFLEX S flow cytometer. Due to a defect of the BD FACSCanto II, the measurements of the cell line SW620 for the uptake of particles after 1, 3, 6 and 24 hours and SW480, regarding the uptake of the particles after 1, 3 and 6 hours, were performed with the CytoFLEX S. FSC, SSC, PE - and FITC - fluorescence were recorded. For the detection of the red and green

fluorescence of the 1.14 µm and 0.235 µm PS particles following laser and fluorescent channels were used (see Table 5):

Table 5. Laser and fluorescence channels used to detect PS particles

	Laser specification	**Fluorescent channels**
BD FACSCanto II		
1.14 µm PS particles	Blue 488 nm laser	585/42 BP (PE)
0.235 µm PS particles	Blue 488 nm laser	530/30 BP (FITC)
CytoFLEX S		
1.14 µm PS particles	Yellow 561 nm laser	585/42 BP (PE)
0.235 µm PS particles	Blue 488 nm laser	525/40 BP (FITC)

All experiments were performed in duplicate and each sample was measured three times, analysing 10.000 events each. Controls of cells without particles in the same conditions were done as well. To exclude cellular aggregates from the analyses, doublet discrimination was performed by plotting the side scatter – area (SSC-A) against the side scatter – height (SSC-H). Flow cytometry data was evaluated using Flowing Software 2 (Turku Bioscience, University of Turku and Åbo Akademie University, Turku, Finland, 2013).

4. Results

4.1 Effect of particle size on MNP uptake

Fluorescence microscopy was used to qualitatively evaluate particulate uptake by four different colon cancer cell lines HT29, HCT116, SW480 and SW620. Bright field and fluorescence images were captured after 24 hours of exposure to 10, 1, 0.1, 0.01 and 0.001 µg/ml PS particles at 37°C. Figure 7 shows all four cell lines exposed to the 9.55, 1.14 and 0.235 µm PS particles at a concentration of 1 µg/ml. To illustrate the results, the concentration of 1 µg/ml was chosen because few to no particles were visible in the lower range and a higher concentration of 10 µg/ml represented an overload. Images of the remaining concentrations can be found in Appendix A.

As assumed, the 9.55 µm particles were not absorbed by any of the four cell lines due to their size and only partially deposited around the cell layers. Since the cells of the four cell lines themselves only have a size of 10 to approximately 20 µm (measuring method: microscope, ImageJ), an uptake of almost 10 µm particles seems very unlikely. The 1.14 and the 0.235 µm particles have shown to accumulate in the cells or on the cell surface, following an increased cellular accumulation trend at higher concentrations (see Appendix A). Particle accumulation of these PS particles was evident in each of the four cell lines, but distinct differences were observed in the respective colon cancer cell lines. Both, the 1.14 and the 0.235 µm particles, show the highest degree of accumulation in the HCT116 and SW480 cells, whereas in the HT29 and SW620 cells only a very low accumulation was observed, even at extremely high concentrations. For 1.14 µm PS particles, many particles surrounded the HT29 and SW620 cells, but only a small fraction was detected in/on the cells. For 0.235 µm PS particles, the same observations were made in HT29 and SW620 cells, at least at very high concentrations (10 µg/ml). Both 1.14 and 0.235 µm particles tend to form aggregates and agglomerates, with the 0.235 µm particles appearing to form larger ones. This experiment demonstrated that 1.14 and 0.235 µm PS particles were indeed associated with the cells. However, a differentiation between cell adhesion and internalization could not be determined from these studies. Further assumptions can only be made by means of additional analytical methods, such as flow cytometry, and not solely on the basis of microscopic assessment.

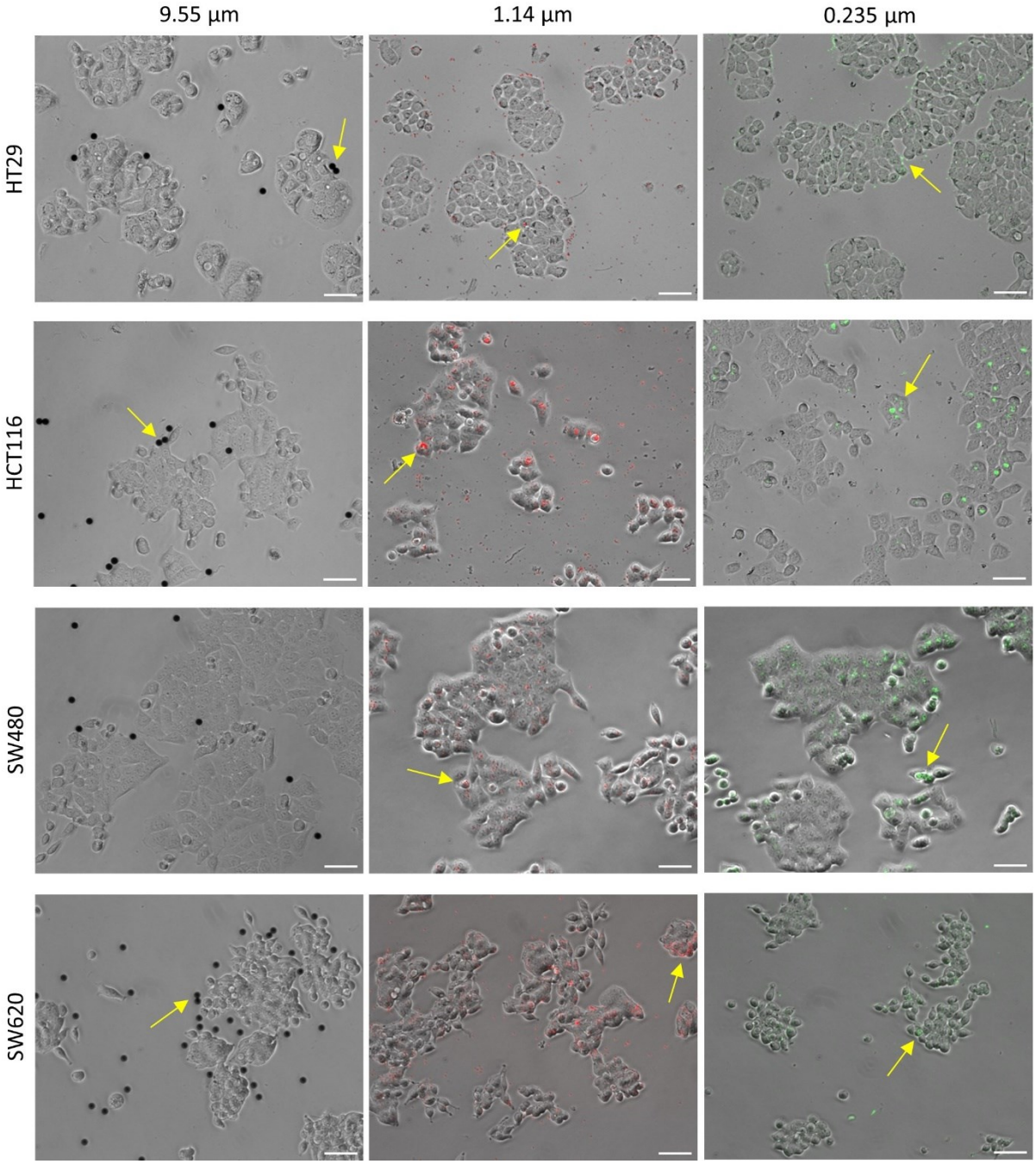

Figure 7. Size-dependent uptake of PS-MNP particles by HT29, HCT116, SW480 and SW620 colon cancer cells. Analysis was performed using inverted fluorescence microscopy after exposure to 1 µg/ml PS 9.55, 1.14 and 0.235 µm particles for 24 hours. Brightfield images of blue coloured 9.55 µm particles (left), multichannel fluorescence images of red fluorescent 1.14 µm (middle), and green fluorescent 0.235 µm (right) PS particles. Yellow arrow: PS-MNP particle accumulation. Scale bars: 50 µm.

4.2 Intracellular localisation of PS-MNP particles

Confocal microscopy was applied to further differentiate between internalization and cell adhesion and to localize the PS particles inside the cells. Due to the results of the previously performed fluorescence microscope studies, further imaging experiments were limited to the 1.14 and 0.235 µm PS particles. To investigate PS-MNP particle internalization HT29, HCT116, SW480 and SW620 cells were exposed to 1 µg/ml of fluorescent 1.14 and 0.235 µm particles for 24 hours at 37°C.

To determine the exact localization of the internalized PS particles, the nucleus was stained with Hoechst 33342 (blue), lysosomes were stained with LysoTracker Deep Red (red) and endosomes with a primary EEA1 antibody and an Alexa Fluor 633 – conjugated secondary antibody (red).

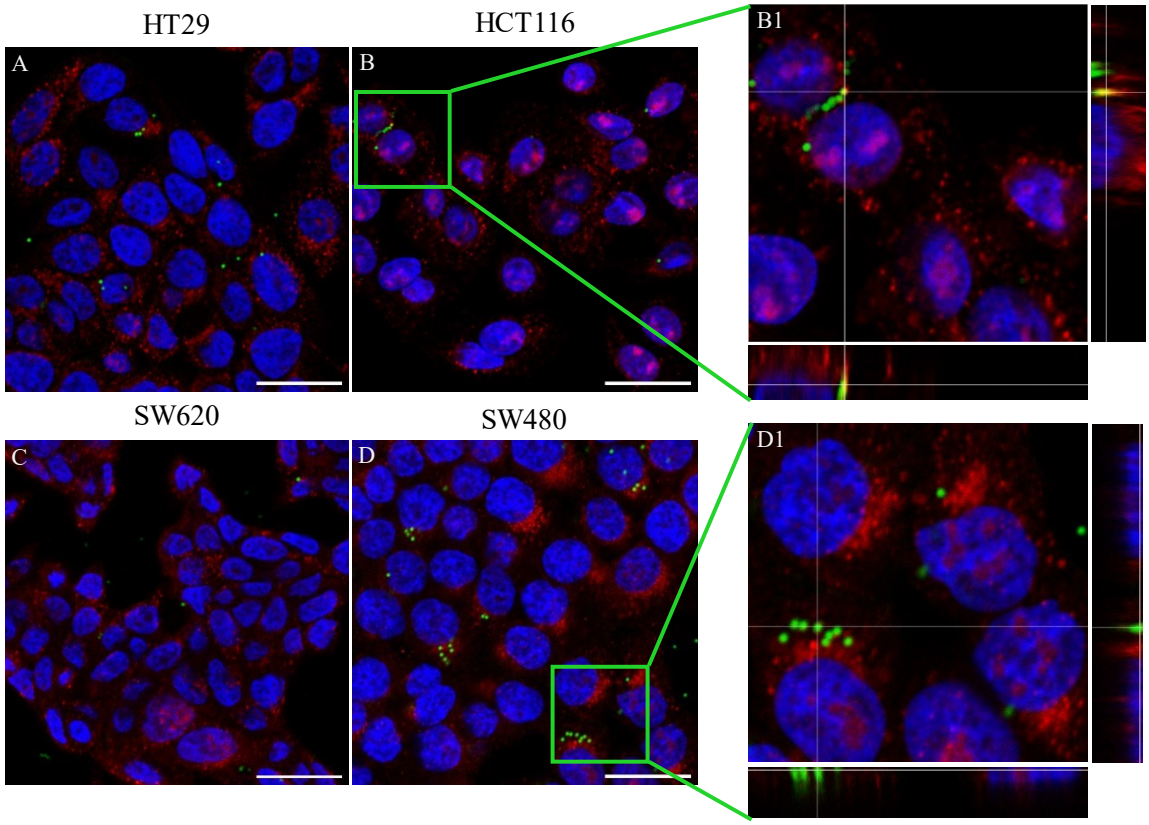

Figure 8. Cellular internalization and localization in endosomes of 1.14 µm PS particles. CLSM images A-D correspond to HT29, HCT116, SW480 and SW620 cells exposed to 1 µg/ml of the PS particles. Images B1 and D1 show a projection through the z-stack. Nuclei are stained in blue, endosomes in red and 1.14 µm PS particles are shown in green. Yellow is the merged fluorescence from PS particles and endosomes. Scale bars: 30 µm.

Figure 8 shows the CLSM images of all four cell lines incubated with red fluorescent 1.14 µm PS particles (shown in green). The 1.14 µm PS particles show co-localization with

endosomes in HCT116 cells, indicated by the merged fluorescence (yellow) of the PS particles and endosomes (Figure 8B, B1). In contrast, none of the 1.14 µm particles were detected in the endosomes of the other three cell lines (Figure 8A, C, D, D1). However, an accumulation of the 1.14 µm particles to the extent seen in the fluorescence microscope images is not discernible.

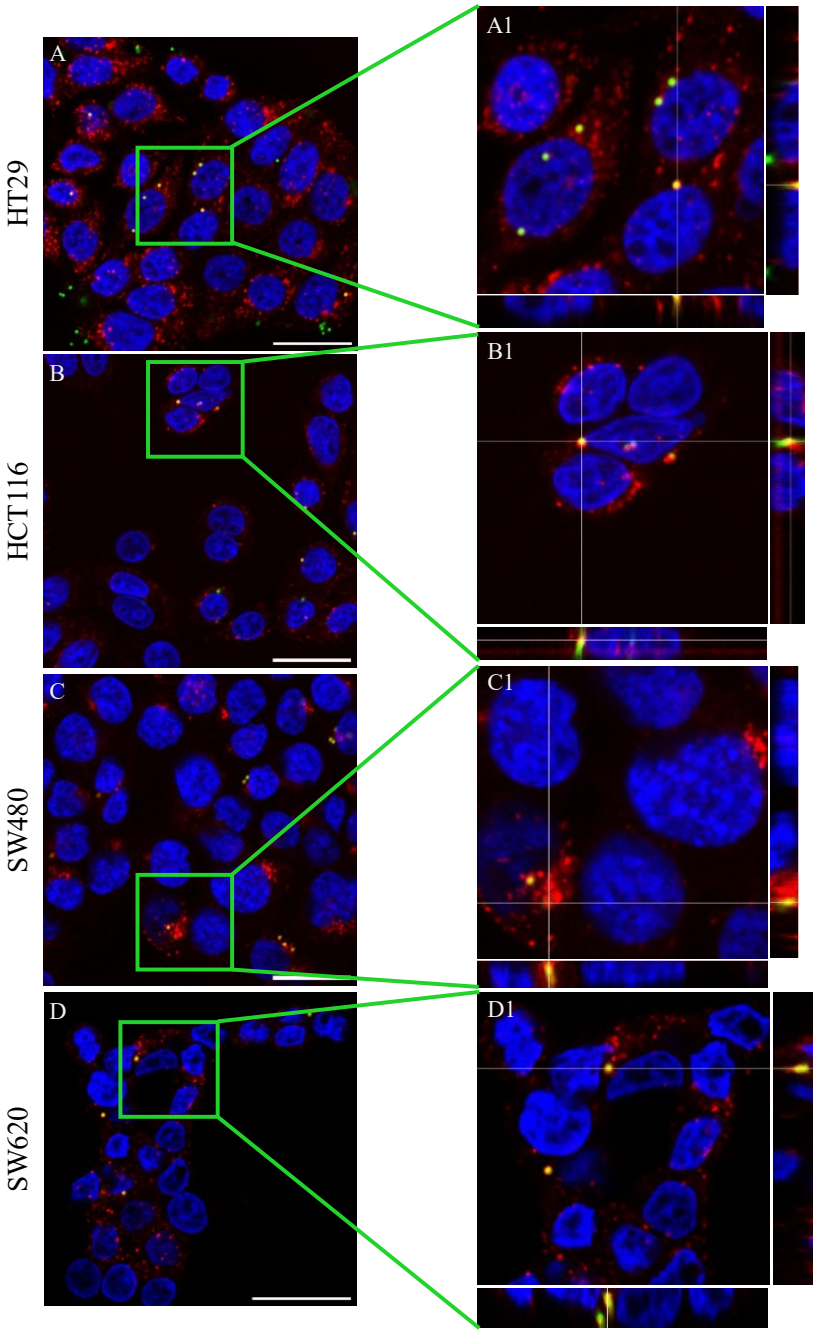

Figure 9. Cellular internalization and localization in lysosomes of 1.14 µm PS particles. CLSM images of HT29, HCT116, SW480 and SW620 cells after 24 hours of exposure to 1 µg/ml 1.14 µm PS particles (A-D) and orthogonal projections of z-stacks of each cell line (A1-D1). Nuclei are stained in blue, lysosomes in red and 1.14 µm PS particles appear in green. The merged fluorescence of PS particles and lysosomes is yellow. Scale bars: 30 µm.

As shown in Figure 9, the 1.14 µm PS particles exhibit co-localization with lysosomes in all four colon cancer cell lines. Again, confirmed by the yellow fluorescence showing an overlap of PS particles and lysosomes. The results of CLSM experiments indicate that the internalized 1.14 µm PS particles are mainly distributed in the lysosomes.

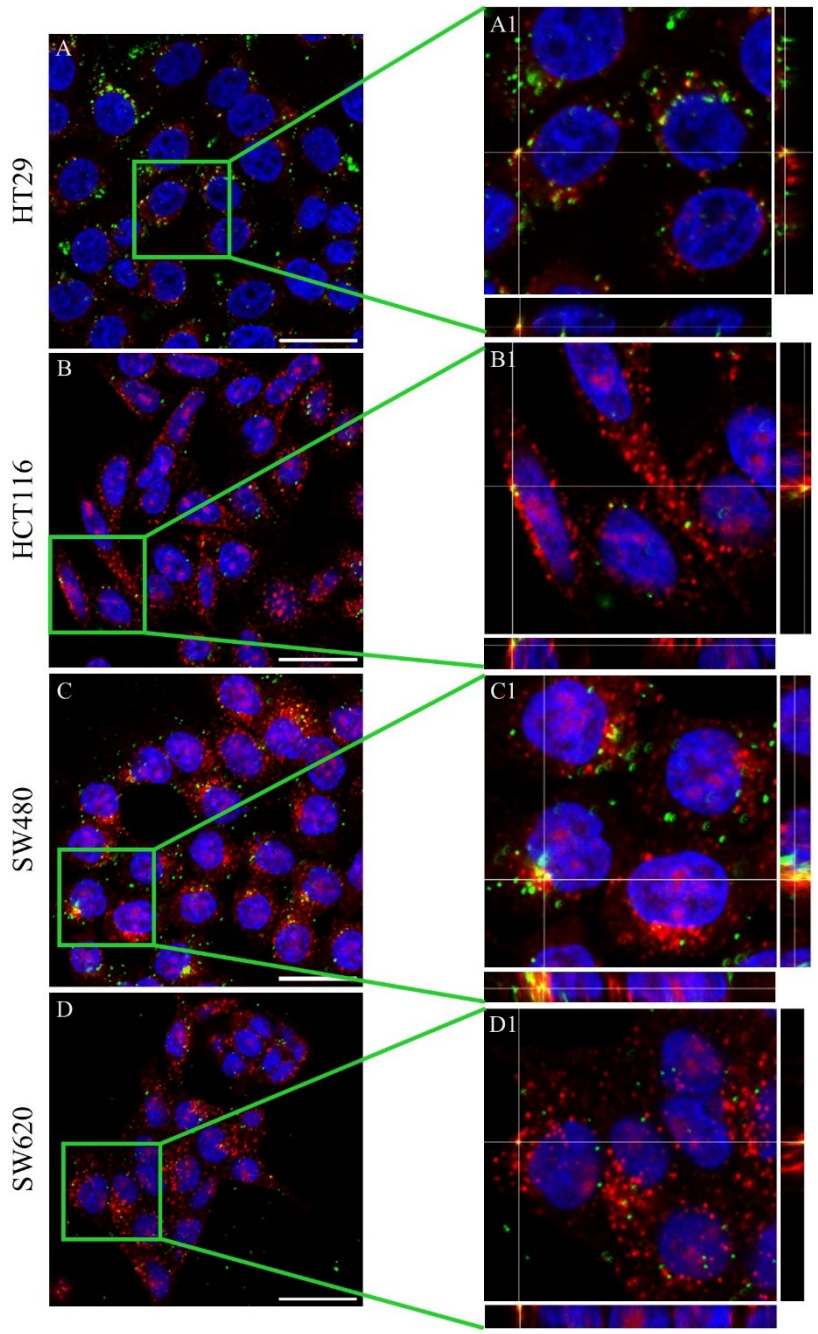

Figure 10. Cellular internalization and localization in endosomes of 0.235 µm PS particles. CLSM Images on the left represent HT29, HCT116, SW480 and SW620 cells exposed to 1 µg/ml 0.235 µm PS particles (A-D) while images on the right (orthogonal projections of z-stacks) correspond to the zoomed area, as indicated by green squares (A1-D1). Nuclei are stained in blue, endosomes in red and 0.235 µm PS particles appear in green. Yellow is the merged fluorescence of PS particles and endosomes. Scale bars: 30 µm.

Intracellular particle uptake in the HT29, HCT116, SW480 and SW620 cells was also evident for 0.235 µm PS particles. For 0.235 µm PS particles an overlap of the PS particles and the endosomes was observed as well, as shown in the orthogonal view of the z-stacks (Figure 10 A1-D1). However, in contrast to the 1.14 µm particles, they were found in the endosomes of all four colon cancer cell lines.

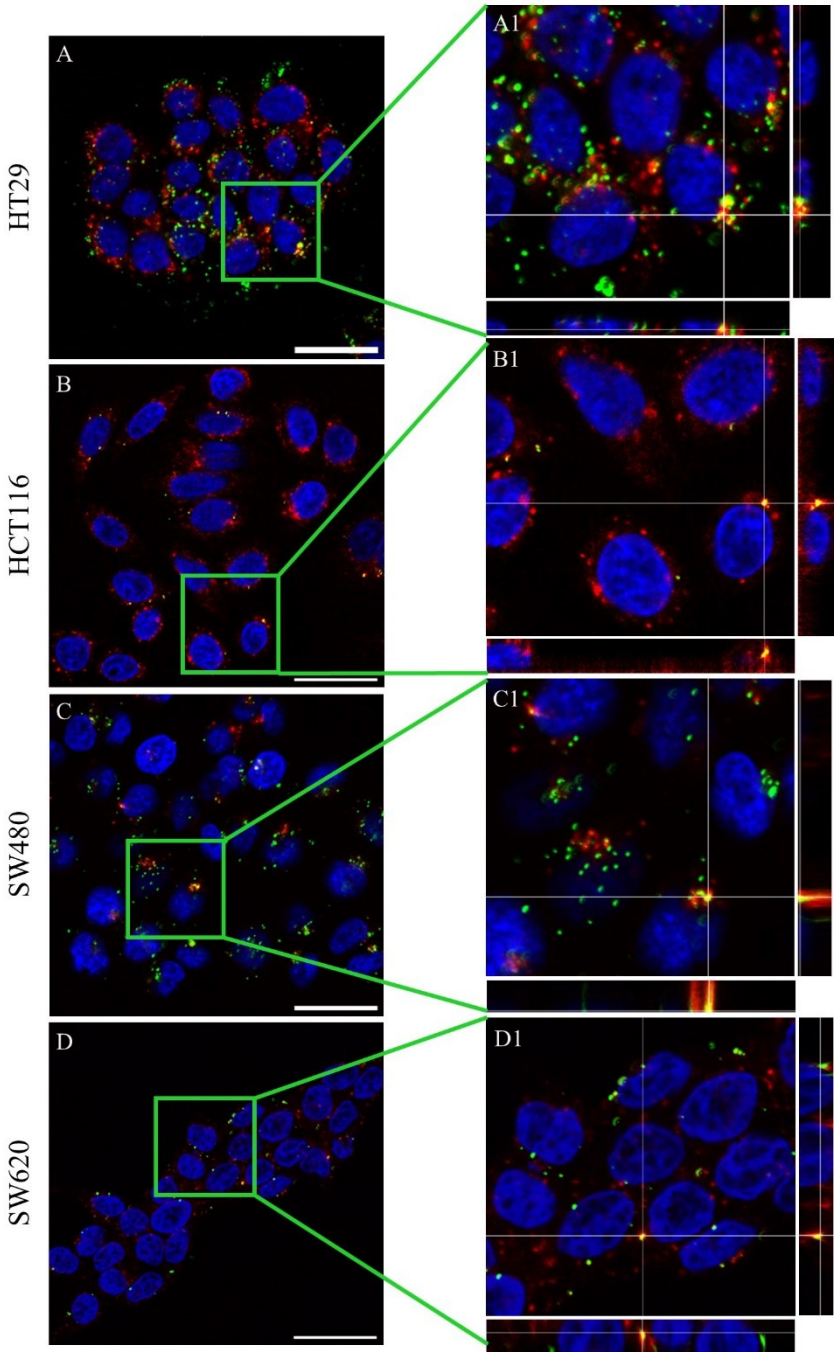

Figure 11. Cellular internalization and localization in lysosomes of 0.235 µm PS particles. CLSM Images of HT29, HCT16, SW480 and SW620 cells after exposure to 0.235 µm PS particles for 24 hours (A-D). Images A1-D1 show the orthogonal projections of z-stacks of each cell line. Nuclei stained in blue, lysosomes in red and PS particles are shown in green. Yellow is the merged fluorescence of PS particles and lysosomes. Scale bars: 30 µm.

As shown in Figure 11, 0.235 µm PS particles were also found inside the lysosomal compartments of HT29, HCT116, SW480 and SW620 cells. Internalization and co-localization with the lysosomes were again confirmed by z-stack imaging (Figure 11 A1 - D1).

Accumulation of 0.235 µm PS particles observed in fluorescence microscopy experiments was confirmed by CLSM imaging. CLSM images (Figure 12) show that 0.235 µm PS particles do not only accumulate on the surface or in the cytoplasm of the cells, but also in the lysosomes and endosomes. Furthermore, Figure 12 shows that the 0.235 µm PS particles tend to form aggregates within the cell, including in the lysosomes and endosomes.

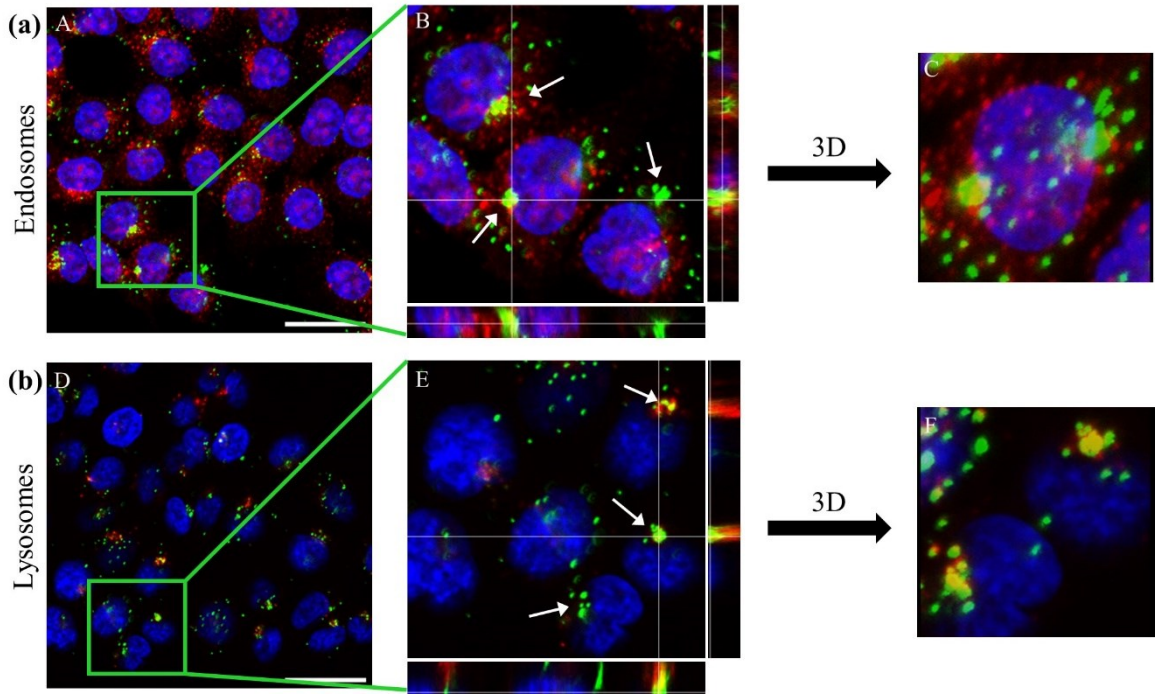

Figure 12. Accumulation of 0.235 µm PS particles in colon cancer cells. Representative CLSM images of SW480 cells incubated with 1 µg/ml 0.235 µm PS particles (A, D). Image B and E show an enlarged area of image A and D, highlighted by a green square. Image C and F show three-dimensional reconstructed images. Nuclei are stained in blue, endosomes (a) and lysosomes (b) in red. PS particles are depicted in green. The yellow fluorescence shows the overlap of PS particles and endosomes/lysosomes. Accumulation of particles and their formation of aggregates is indicated by white arrows. Scale bar: 30 µm.

Overall, the internalized PS-MNP particles appear to partially surround the nuclei, although it is unclear whether the particles are inside the nuclei or not. To verify this, orthogonal projections (Figure 13) and three-dimensional images (data not shown) of the Z-stacks were created. As expected, there was no evidence of particle uptake into the nucleus for 1.14 µm PS particles. In contrast, particle adhesion of 0.235 µm PS particle on the nuclear membrane

is visually evident (Figure 13B, D). In addition, 0.235 µm particles were also detected within the cell nuclei (Figure 13A, C).

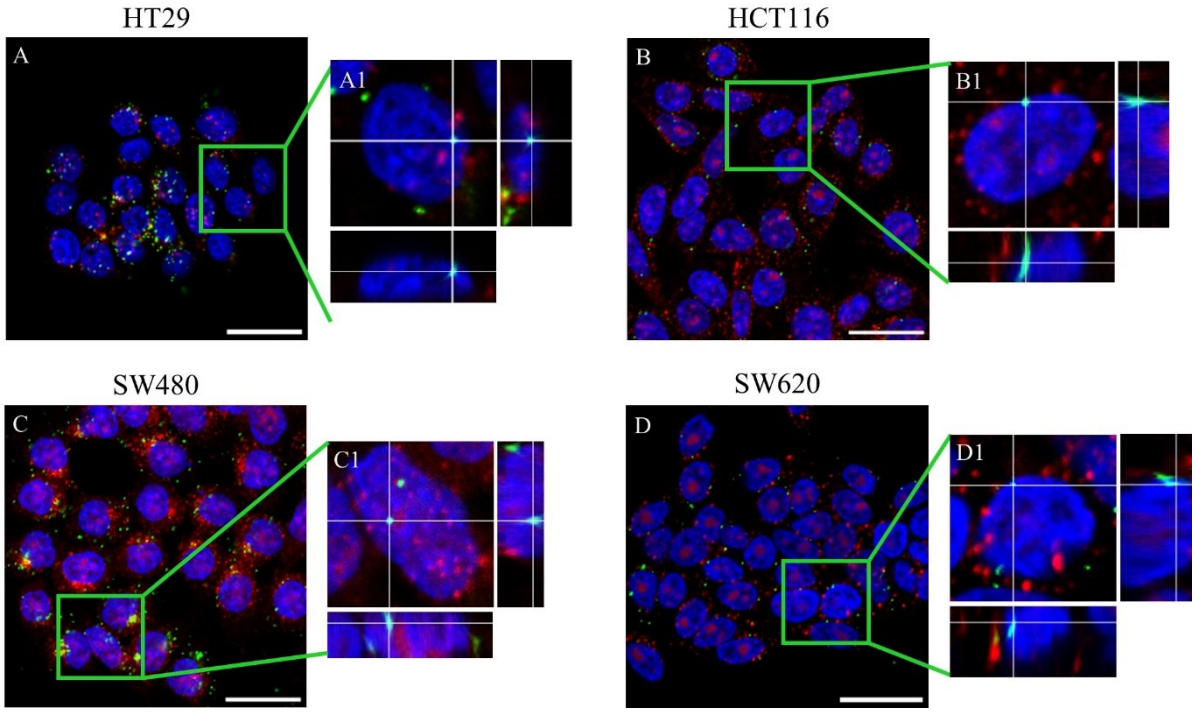

Figure 13. CLSM images demonstrate the presence of 0.235 µm PS particles inside cell nuclei. Images A-D show HT29, HCT116, SW480 and SW620 cells incubated with 1 µg/ml 0.235 µm PS particles for 24 hours. Images A1, B1, C1 and D1 show a zoomed area of images A, B, C and D, respectively, as highlighted by the green squares. Nuclei are stained in blue, endosomes in red and 0.235 µm particles appear in green. The light blue fluorescence shows the overlap of PS particles and nuclei. Scale bars: 30 µm.

4.3 Quantification of MNP particle uptake in cells

To ascertain the internalization efficiency of 1.14 and 0.235 µm PS particle by HT29, HCT116, SW480 and SW620 flow cytometry was used. In order to observe an increase of particle uptake, a kinetic study was performed and samples were taken after 1, 3, 6 and 24 hours. The fluorescently labelled 1.14 and 0.235 µm particles can be detected inside the cell by showing a higher fluorescence than cells without particles. Since the fluorescence of the particles is additive, the intensity of intracellular fluorescence indicates the amount of internalized particles. Intracellular 1.14 µm particles were measured as double positive signals, since they showed fluorescent activity not only in the red (PE) but also in the green channel (FITC), whereas the 0.235 µm particles were only fluorescently active in the green channel as illustrated in Appendix B.

In the kinetic study, the mean fluorescence and thus the proportion of particle-positive cells increased in all four cell lines exposed to 1 µg/ml of 1.14 and 0.235 µm PS particles over a period of 24 hours (Figure 14). The highest uptake rates after 24 hours were determined for HCT116 cells for both PS 1.14 and 0.235 µm particles. The uptake of PS 1.14 µm was quantified at 50.9% and for PS 0.235 µm at 89.5%. In addition, HCT116 cells already show an extremely high uptake rate of 0.235 µm particles (73.2%) after 6 hours compared to the other cell lines (HT29 29.3%; SW480 39.9%; SW620 26%) (Figure 13D). Interestingly, SW620 cells showed no to very low uptake of 1.14 µm particles in the first 6 hours (Figure 14A and C). However, after 24 hours the amount of internalized particles increased rapidly and was therefore 37 times higher than after 6 hours. In contrast, this uptake behaviour of SW620 cells was not observed for PS 0.235 µm (Figure 14B and D).

Furthermore, it was possible to clearly identify cell populations with different numbers of particles by separate peaks in fluorescence intensity histograms (Appendix C). However, it should be noted that this was only possible for 1.14 µm PS particles. Direct quantification of the numbers of particles interacting per cell was not possible for the 0.235 µm PS particles. Instead of individual and clearly identifiable populations, the total fluorescence distribution changed only to higher values in an approximately wider peak. This is probably due to a lack of resolution of the flow cytometer. As shown in Figure 14, the number of 1.14 µm PS particles taken up by a cell increased in a time dependent manner. After 1, 3 and 6 hours of incubation, for the most part only 1 particle per cell has been taken up in all four cell lines and no to very few cells have internalized 2, 3 or > 4 particles. However, it is also clear that with longer incubation times, cells absorb an increasing number of particles. After 24 hours,

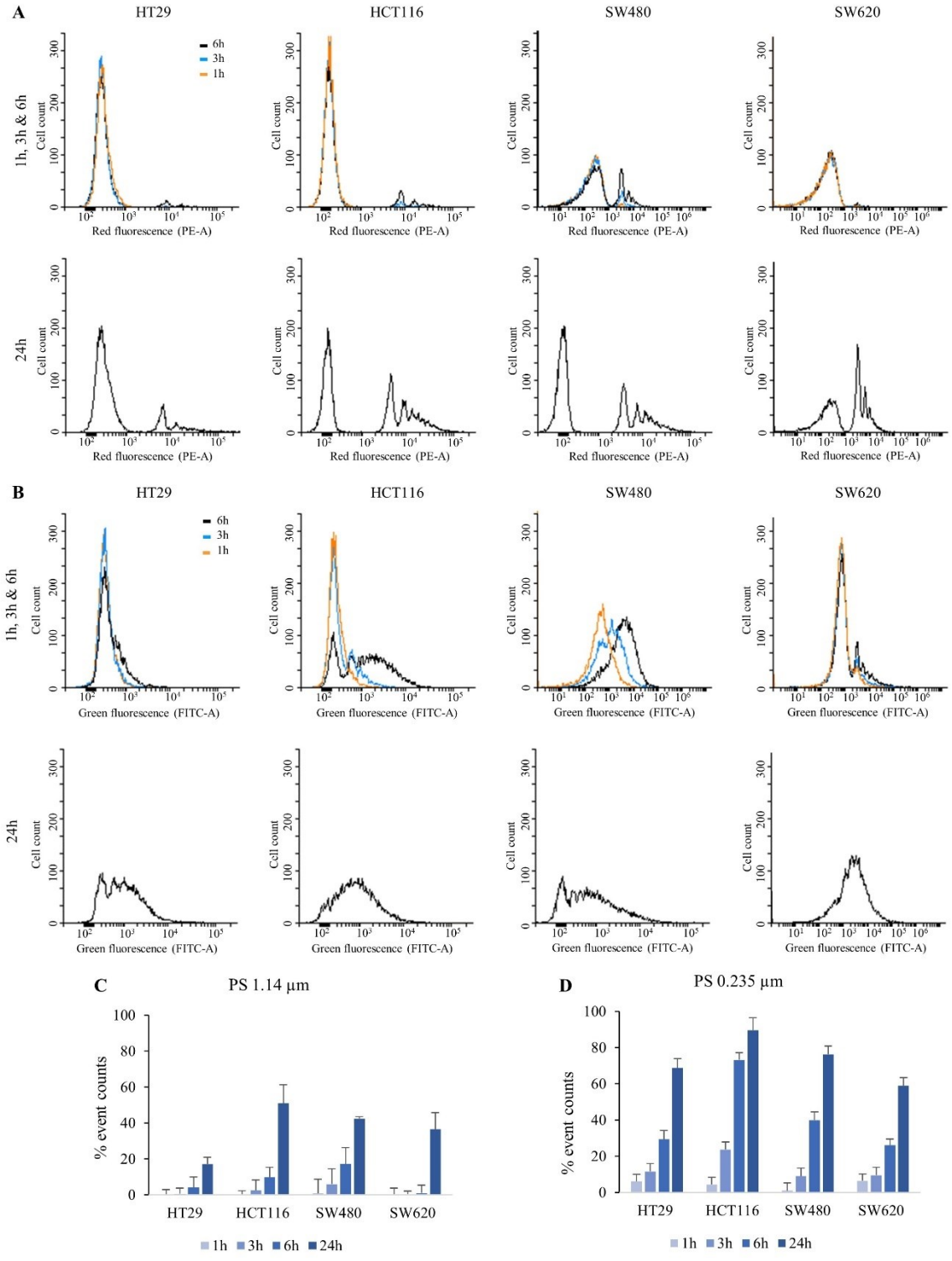

Figure 14. Uptake of 1.14 µm and 0.235 µm PS particles in colon cancer cells after 1, 3, 6 and 24 hour incubation. Fluorescence intensity histograms of HT29, HT116, SW480 and SW620 cells exposed to 1 µg/ml of 1.14 µm (A) and 0.235 µm (B) PS particles. The percentage of particle-positive cells over the total cell population is presented in figure C for 1.14 µm and D for 0.235 µm particles. Data are shown as means ± standard deviation (SD).

12.37, 10.83 and 3.21% of HCT116, SW480 and SW620 cells had taken up more than 4 particles per cell respectively and 4.14% of HT29 cells more than 3 particles per cell.

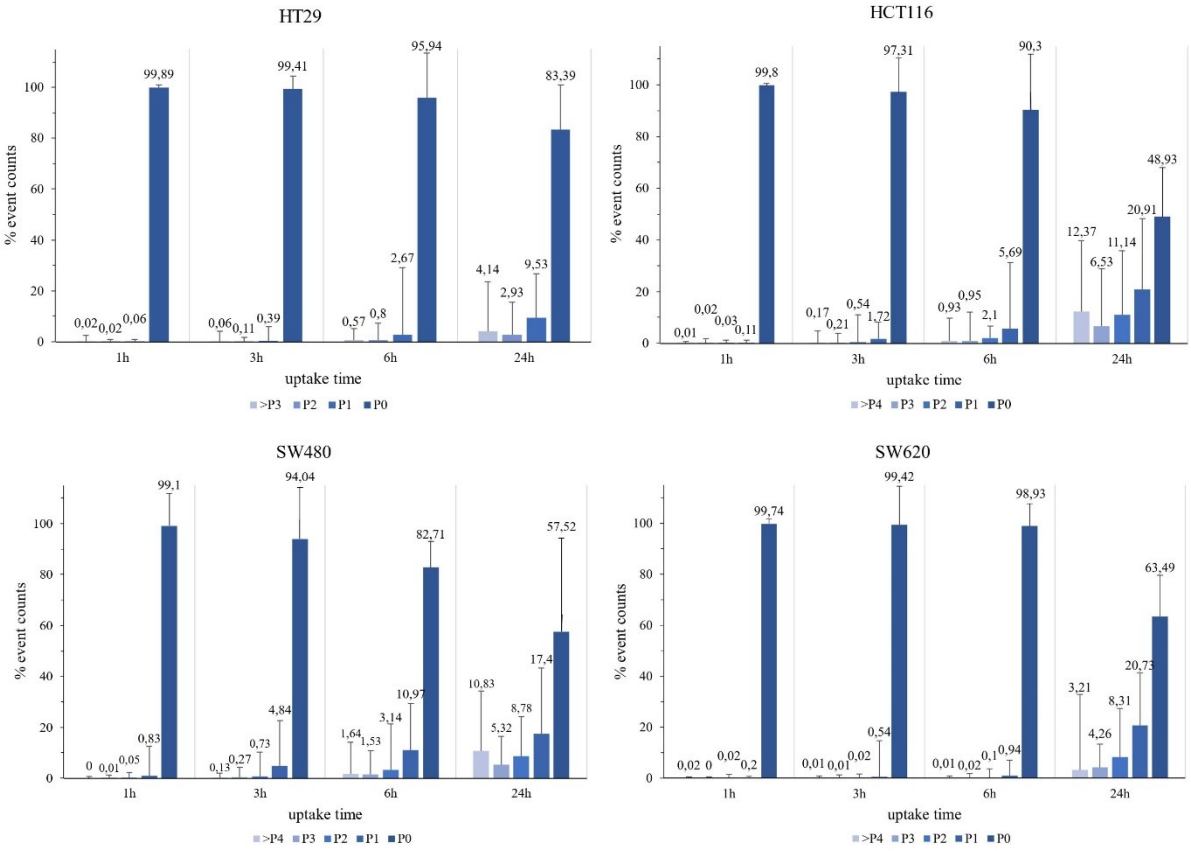

Figure 15. Identification of cell populations with different numbers of internalized 1.14 µm PS particles. Values given in the bar graphs show the percentage of particle-positive cells. The abbreviations P0, P1, P2, P3 and >P4 correspond to cells that have not taken up any particles, one, two, three or four or more particles, respectively. Data represent mean ± SD.

In addition to the kinetic studies, 24 hour uptake experiments were conducted with 3 different concentrations (0.1, 1 and 10 µg/ml) of the 1.14 and 0.235 µm PS particles. As shown in Figure 15, both PS particles sizes were found to accumulate in all four colon cancer cell lines in a dose-dependent manner. This observation is consistent with the results of fluorescence microscopy. At low concentrations (0.1 µg/ml), the 1.14 µm PS particles showed almost no interactions with the two cell lines HT29 (3.5%) and SW620 (5.8%) (Figure 15A). For HCT116 (12.3%) and SW480 (11.6%) cells, slightly higher interaction rates were observed with 1.14 µm particles. In contrast, particle-cell interactions were clearly detected at higher concentrations of 1 and 10 µg/ml. The highest interaction rates were observed again in HCT116 cells. At concentrations of 1 and 10 µg/ml, 51.1 and 85.8% of HCT116 and 42.4 and 76,1% of SW480 cells showed interaction with the 1.14 µm particles,

respectively. HT29 cells showed the lowest interactions for 1.14 µm particles with 16.6% at 1 µg/ml and 42.1% at 10 µg/ml compared to the other 3 cell lines. Furthermore, it was observed that HCT116 and SW480 cells had an extremely high percentage (61.3 and 51.3%, respectively) of cells that absorbed more than 4 particles per cell (illustrated in Appendix C). A detailed representation of the number of 1.14 µm PS particles interacting per cell can be found in Appendix C for each cell line. The general tendency for particle-cell interactions was by far higher for 0.235 µm particles, as shown in Figure 15B. Even at low concentrations of 0.1 µg/ml, uptake rates of up to 41.7% (for HCT116) were observed. The uptake of 0.235 µm particles in HCT116 cells even increased to 98.5% at concentrations of 10 µg/ml.

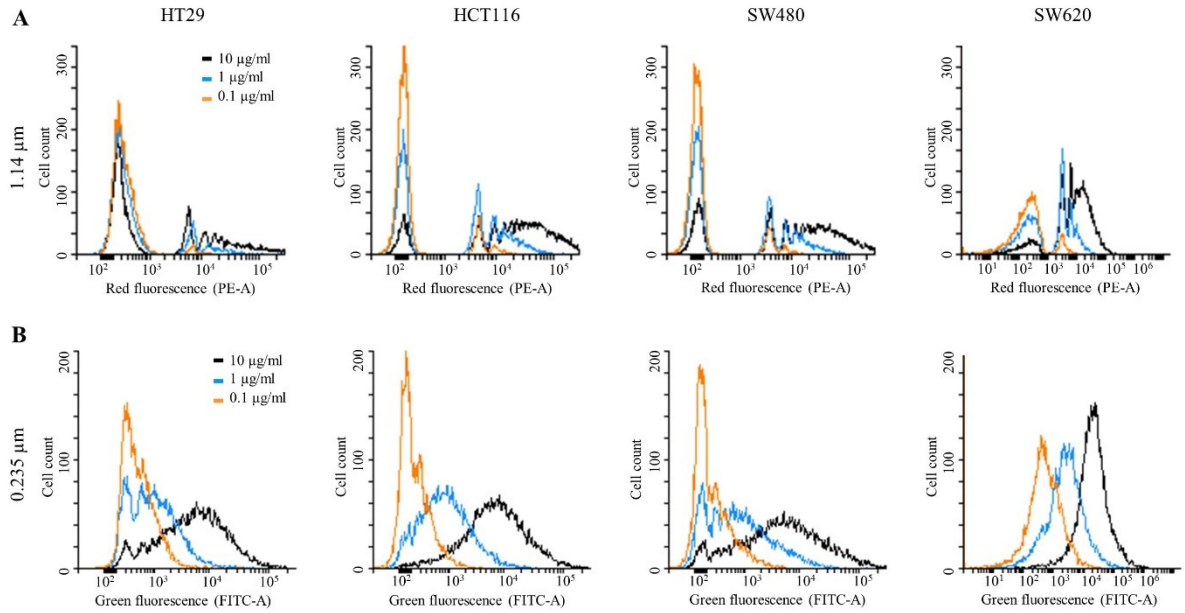

Figure 16. Accumulation of 1.14 and 0.235 µm PS particles in a dose-dependent way. Fluorescence intensity histograms of HT29, HCT116, SW480 and SW620 cells exposed to 3 different concentrations (0.1, 1 and 10 µg/ml) of 1.14 (A) and 0.235 µm (B) PS particle for 24 hours at 37°C.

5. Discussion

Plastic is ubiquitous, not only in our society but also in our environment and therefore leads to an inevitable human exposure. The contamination of food with MNP is of particular concern. Due to ingestion of contaminated foods, the human GIT is most likely the first site of exposure to MNP on a daily basis (Hwang et al., 2020; Visalli et al., 2021). Therefore, the aim of this work was to investigate the interaction between different PS-MNP particles and four colon cancer cell lines, including the determination of the influence of particle size on cellular internalization, the localization of MNP particles in cellular compartments and the quantification of cellular uptake. Similar to the majority of studies conducted so far, spherical PS particles were used in this work. This represents a limitation, not only because PS is one of many polymer types, but also because pristine PS-MNP particles have been used and thus do not correspond to the naturally occurring MNPs in the environment. In the environment, MNP particles are more diverse and complex, not only in terms of polymer type and size, but also in their shape, as they are random shaped and weathered by different environmental influences.

Four different colon cancer cell lines were chosen to represent a model of cancer progression and to investigate whether the aggressiveness of the respective cell line has an impact on particle uptake. According to their elastic modulus, SW620 cells are more deformable and softer than SW480 cells (Armistead et al., 2020) and should therefore, with regard to the assumption of Brill-Karniely et al., have a higher particle uptake (Brill-Karniely et al., 2020). Interestingly, SW620 cells showed a lower uptake after 24 hours for both 1.14 and 0.235 µm PS particles than the SW480 cells. This is in contrast to the reports of Brill-Karniely et al., who observed a higher particle uptake in the highly metastatic subpopulations (PC3M-LN4) with higher mechanical deformability than in the primary prostate cancer cells (PC3M-P) (Brill-Karniely et al., 2020). Since HT29 is derived from a primary adenocarcinoma with Duke's Stage C and has a similar elastic modulus as the SW620 (Armistead et al., 2020), it was assumed that particle uptake in this cell line would be higher than in SW480 cells isolated from a Duke's Stage B primary adenocarcinoma. However, the observations of this study contradict this hypothesis, because after 24 hours of incubation the HT29 cells showed the lowest uptake of 1.14 µm PS particles compared to other cell lines. Moreover, lower uptake rates of 0.235 µm PS particles into HT29 cells were observed compared to SW480 cells. HCT116 cells, on the other hand, showed the highest uptake rates for both 0.235 and 1.14 µm PS particles. Since there is no uniform classification of the HCT116 cell line in the

literature regarding its cancer aggressiveness, it is difficult to relate the results of HCT116 cells to those of other cell lines. A possible explanation why this cell line shows the highest uptake rates could be that they belong to the mesenchymal consensus molecular subtype 4 (CMS4) (Berg et al., 2017). CMS4 may be more aggressive than other CMS subtypes due to upregulation of genes involved in epithelial mesenchymal transition (EMT) and signatures related with the activation of transforming growth factor β (TGFβ) (Guinney et al., 2015). In all four cell lines a substantial uptake of the 1.14 µm and especially of the 0.235 µm PS particles was shown, whereas no uptake of the 9.55 µm particles was observed. This result is in line with previous reports in which the upper limit of intracellular MNP uptake in intestinal epithelial cells was set at 10 µm (Bruinink et al., 2015). Furthermore, this work has shown that cellular interaction and uptake increase with decreasing particle size, which is consistent with the results of Shi et al., who found that nano-sized PS particles are more easily absorbed than micro-sized PS particles (Shi et al., 2022). On the other hand, it must be noted that there are also differences in the range of nano-sized or micro-sized particles. Kulkarni et al. showed that 100 nm PS particles had higher uptake rates in Caco-2 cells than other particle sizes, such as 25, 50, 200 and 500 nm. Therefore, medium-sized particles with sufficient adhesion energy to cover the required energy associated with the bending of the membrane and the membrane tension are ideal for uptake into the cell (Kulkarni and Feng, 2013).

The uptake of 1.14 and especially 0.235 µm was widespread, with particles found inside the cells where they co-localized with lysosomes and endosomes. With CLSM, it was possible to observe the accumulation of 0.235 µm PS particles, especially in lysosomes. In fact, it has been shown that accumulation of amine-modified PS particle at the nanoscale can damage lysosomes, leading to a release of lysosomal content (e.g. cathepsins) into the cytosol and further to apoptosis (Wang et al., 2013). Although 1.14 µm PS particles also co-localized with the lysosomes as shown in the CLSM images, no accumulation was observed. One possible explanation for this could be that larger particles in the micrometre scale may escape from the lysosomes into the cytosol after endocytosis (Llorca and Farré, 2021; Wu et al., 2019). However, lysosomal leakage could not be confirmed by the study of Seydoux et al., in which 1 µm PS particles showed co-localization with lysosomes in bone marrow-derived dendritic cells (BMDCs) (Seydoux et al., 2014).

Besides their localization in the cytoplasm, lysosomes and endosomes, 0.235 µm PS particles were detected on the nuclear membrane as well as in the nuclei themselves. This is in contrast

with most literature reports, where uptake into the cell nucleus was observed only for particles < 50 nm. Since nanoparticles must be extremely small to pass either passively through the nuclear pore complex (~6-9 nm) or actively through the nuclear membrane pore complex (<50 nm) (Augustine et al., 2020), only the widely accepted hypothesis that nanoparticles enter the nucleus during cell division (Fröhlich, 2012) could explain the localization of the 0.235 µm PS particles in the nuclei.

Overall, the results of this work clearly show that both micro- and nanoplastic particles can enter the cells, whereby the uptake rates of MNP particles depend on both the particle size and the cell type/cell line. Since the manufacturer has not provided any information on the charge of the particles and no particle characterisation has been performed within the scope of this study, further studies on this parameter are necessary. Especially since the charge of the particles do not only influences internalisation, but also plays an important role in terms of toxicity. Inkielewicz-Stepniak et al., reported that positively charged NPs strongly interacted with mucin leading to an aggregation of the mucin chains, whereas negatively charged NPs did not induce mucin aggregation (Inkielewicz-Stepniak et al., 2018). However, going forward, it will be important to consider the involvement of the gastrointestinal mucus layer with regard to MNP toxicity.

6. Conclusion

In summary, the interaction between PS-MNP particles and colon cancer cells, including the particle uptake and the intracellular fate of PS particles was investigated in this work.
It was found that particle size plays a decisive role, not only in terms of whether particles are absorbed at all, but also to what extent this occurs. Hence, it was shown that 9.55 µm PS particles are not taken up by any of the four cell lines. PS 1.14 and 0.235 µm particles, on the other hand, are well absorbed by all four cell lines, with differences between the cell lines being observed. Regardless of the different uptake rates between the cell lines themselves, the highest uptake rates for both particle sizes are shown for the HCT116 cell line. Both particle sizes accumulate in all four colon cancer cell lines in a concentration dependent manner, with very high uptake rates for 0.235 µm particles even at the lowest concentration.
The interaction of 1.14 and 0.235 µm PS particles with the colon cancer cells was not limited to membrane adhesion only. The incorporation of these particles in the cells was first implied by fluorescence microscopy and confirmed by CLSM. Using qualitative CLSM analysis, the fluorescently labelled PS particles were detected within the cells and localized in both the lysosomes and the endosomes. However, 1.14 µm particles were localized only in the lysosomes. In contrast to 0.235 µm particles, no uptake of 1.14 µm particles into the endosomes was observed, with the exception of HCT116 cells. Particle adhesion to the nuclear membrane and uptake into the nucleus itself, was observed for 0.235 µm particles.

Further studies are needed to investigate the influence of parameters such as particle size, shape, material or surface charge. Other MNP types such as PE, PP, PVC or PET may behave differently from PS. Moreover, not only the particle size but also the surface charge influences the cellular interaction as well as the toxicity and accumulation of the particles. Since both the 1.14 and 0.235 µm PS have been partially absorbed by the cells to a very high extent, further studies on the accumulation and toxicity of the particles are necessary.
In summary, the present work provides a solid basis of knowledge regarding the interaction of PS particles with human epithelial colon cancer cells, the uptake behaviour and the intracellular fate of MNP particles in these cells.

7. References

Adan, A., Alizada, G., Kiraz, Y., Baran, Y., Nalbant, A., 2017. Flow cytometry: basic principles and applications. Critical Reviews in Biotechnology 37, 163–176. https://doi.org/10.3109/07388551.2015.1128876

Ahmed, D., Eide, P.W., Eilertsen, I.A., Danielsen, S.A., Eknæs, M., Hektoen, M., Lind, G.E., Lothe, R.A., 2013. Epigenetic and genetic features of 24 colon cancer cell lines. Oncogenesis 2, e71–e71. https://doi.org/10.1038/oncsis.2013.35

Andrady, A.L., Neal, M.A., 2009. Applications and societal benefits of plastics. Philos Trans R Soc Lond B Biol Sci 364, 1977–1984. https://doi.org/10.1098/rstb.2008.0304

Armistead, F.J., Gala De Pablo, J., Gadêlha, H., Peyman, S.A., Evans, S.D., 2020. Physical Biomarkers of Disease Progression: On-Chip Monitoring of Changes in Mechanobiology of Colorectal Cancer Cells. Sci Rep 10, 3254. https://doi.org/10.1038/s41598-020-59952-x

Augustine, R., Hasan, A., Primavera, R., Wilson, R.J., Thakor, A.S., Kevadiya, B.D., 2020. Cellular uptake and retention of nanoparticles: Insights on particle properties and interaction with cellular components. Materials Today Communications 25, 101692. https://doi.org/10.1016/j.mtcomm.2020.101692

Banerjee, A., Shelver, W.L., 2021. Micro- and nanoplastic induced cellular toxicity in mammals: A review. Science of The Total Environment 755, 142518. https://doi.org/10.1016/j.scitotenv.2020.142518

Behzadi, S., Serpooshan, V., Tao, W., Hamaly, M.A., Alkawareek, M.Y., Dreaden, E.C., Brown, D., Alkilany, A.M., Farokhzad, O.C., Mahmoudi, M., 2017. Cellular uptake of nanoparticles: journey inside the cell. Chem. Soc. Rev. 46, 4218–4244. https://doi.org/10.1039/C6CS00636A

Berg, K.C.G., Eide, P.W., Eilertsen, I.A., Johannessen, B., Bruun, J., Danielsen, S.A., Bjørnslett, M., Meza-Zepeda, L.A., Eknæs, M., Lind, G.E., Myklebost, O., Skotheim, R.I., Sveen, A., Lothe, R.A., 2017. Multi-omics of 34 colorectal cancer cell lines - a resource for biomedical studies. Molecular Cancer 16, 116. https://doi.org/10.1186/s12943-017-0691-y

Brill-Karniely, Y., Dror, D., Duanis-Assaf, T., Goldstein, Y., Schwob, O., Millo, T., Orehov, N., Stern, T., Jaber, M., Loyfer, N., Vosk-Artzi, M., Benyamini, H., Bielenberg, D., Kaplan, T., Buganim, Y., Reches, M., Benny, O., 2020. Triangular correlation (TrC) between cancer aggressiveness, cell uptake capability, and cell deformability. Sci Adv 6, eaax2861. https://doi.org/10.1126/sciadv.aax2861

Bruinink, A., Wang, J., Wick, P., 2015. Effect of particle agglomeration in nanotoxicology. Arch Toxicol 89, 659–675. https://doi.org/10.1007/s00204-015-1460-6

Burkey, T.E., Skjolaas, K.A., Minton, J.E., 2009. BOARD-INVITED REVIEW: Porcine mucosal immunity of the gastrointestinal tract1. Journal of Animal Science 87, 1493–1501. https://doi.org/10.2527/jas.2008-1330

Canton, I., Battaglia, G., 2012. Endocytosis at the nanoscale. Chem. Soc. Rev. 41, 2718–2739. https://doi.org/10.1039/C2CS15309B

Chang, X., Xue, Y., Li, J., Zou, L., Tang, M., 2020. Potential health impact of environmental micro- and nanoplastics pollution. Journal of Applied Toxicology 40, 4–15. https://doi.org/10.1002/jat.3915

Chisanga, D., Keerthikumar, S., Pathan, M., Ariyaratne, D., Kalra, H., Boukouris, S., Mathew, N., Al Saffar, H., Gangoda, L., Ang, C.S., Sieber, O., Mariadason, J., Dasgupta, R., Chilamkurti, N., Mathivanan, S., 2016. Colorectal Cancer Atlas | "HCT116" [WWW Document]. Colorectal Cancer Atlas: An integrative resource for genomic and proteomic annotations from colorectal cancer cell lines and tissue. URL http://www.coloncanceratlas.org/search_cell_line?cell_line=HCT116 (accessed 2.7.23).

Cox, K.D., Covernton, G.A., Davies, H.L., Dower, J.F., Juanes, F., Dudas, S.E., 2019. Human Consumption of Microplastics. Environ. Sci. Technol. 53, 7068–7074. https://doi.org/10.1021/acs.est.9b01517

Daugherty, A.L., Mrsny, R.J., 1999. Transcellular uptake mechanisms of the intestinal epithelial barrier Part one. Pharmaceutical Science & Technology Today 2, 144–151. https://doi.org/10.1016/S1461-5347(99)00142-X

Doherty, G.J., McMahon, H.T., 2009. Mechanisms of Endocytosis. Annu. Rev. Biochem. 78, 857–902. https://doi.org/10.1146/annurev.biochem.78.081307.110540

Donahue, N.D., Acar, H., Wilhelm, S., 2019. Concepts of nanoparticle cellular uptake, intracellular trafficking, and kinetics in nanomedicine. Advanced Drug Delivery Reviews, Unraveling the In Vivo Fate and Cellular Pharmacokinetics of Drug Nanocarriers 143, 68–96. https://doi.org/10.1016/j.addr.2019.04.008

EFSA Panel on Contaminants in the Food Chain (CONTAM), 2016. Presence of microplastics and nanoplastics in food, with particular focus on seafood. EFSA Journal 14, e04501. https://doi.org/10.2903/j.efsa.2016.4501

Fröhlich, E., 2012. The role of surface charge in cellular uptake and cytotoxicity of medical nanoparticles. Int J Nanomedicine 7, 5577–5591. https://doi.org/10.2147/IJN.S36111

Fröhlich, E., Roblegg, E., 2012. Models for oral uptake of nanoparticles in consumer products. Toxicology 291, 10–17. https://doi.org/10.1016/j.tox.2011.11.004

Gompf, A., Dorn-Beineke, A., Frey, O., Klouche, M., Scheffold, A., Bacher, P., Kern, F., Giebel, B., Nebe, C.T., Renz, H., Anderer, U., Savkovic, V., Weiß, R., Schmid, D., Rohde, E., Schiemann, M., Dreher, S., Busch, D.H., Stemberger, C., Hildebrandt, M., Aleksandrova, K., Klöß, S., Arseniev, L., Köhl, U., Odendahl, M., Matko, S., Riewaldt, J., Tonn, T., Sack, U., 2016. Zelluläre Diagnostik und Therapie. De Gruyter, Berlin/Boston.

Guinney, J., Dienstmann, R., Wang, X., de Reyniès, A., Schlicker, A., Soneson, C., Marisa, L., Roepman, P., Nyamundanda, G., Angelino, P., Bot, B.M., Morris, J.S., Simon, I.M., Gerster, S., Fessler, E., de Sousa e Melo, F., Missiaglia, E., Ramay, H., Barras, D., Homicsko, K., Maru, D., Manyam, G.C., Broom, B., Boige, V., Perez-Villamil, B., Laderas, T., Salazar, R., Gray, J.W., Hanahan, D., Tabernero, J., Bernards, R., Friend, S.H., Laurent-Puig, P., Medema, J.P., Sadanandam, A., Wessels, L., Delorenzi, M., Kopetz, S., Vermeulen, L., Tejpar, S., 2015. The Consensus Molecular Subtypes of Colorectal Cancer. Nat Med 21, 1350–1356. https://doi.org/10.1038/nm.3967

Gullberg, E., 2005. Particle Transcytosis Across the Human Intestinal Epithelium : Model Development and Target Identification for Improved Drug Delivery.

HCT.116 Cell Line Details [WWW Document], n.d. . NIH National Cancer Institute - Center for Cancer Research. URL https://strap.nci.nih.gov/celline_detail.php?sample_id=17 (accessed 2.7.23).

Healthcare - Plastics Europe, n.d. . Plastics Europe. URL https://plasticseurope.org/plastics-explained/plastics-in-use/healthcare/ (accessed 11.12.22).

Hesler, M., Aengenheister, L., Ellinger, B., Drexel, R., Straskraba, S., Jost, C., Wagner, S., Meier, F., von Briesen, H., Büchel, C., Wick, P., Buerki-Thurnherr, T., Kohl, Y., 2019. Multi-endpoint toxicological assessment of polystyrene nano- and microparticles in different biological models in vitro. Toxicology in Vitro 61, 104610. https://doi.org/10.1016/j.tiv.2019.104610

Hirt, N., Body-Malapel, M., 2020. Immunotoxicity and intestinal effects of nano- and microplastics: a review of the literature. Part Fibre Toxicol 17, 57. https://doi.org/10.1186/s12989-020-00387-7

Huang, Z., Weng, Y., Shen, Q., Zhao, Y., Jin, Y., 2021. Microplastic: A potential threat to human and animal health by interfering with the intestinal barrier function and changing the intestinal microenvironment. Science of The Total Environment 785, 147365. https://doi.org/10.1016/j.scitotenv.2021.147365

Hwang, J., Choi, D., Han, S., Jung, S.Y., Choi, J., Hong, J., 2020. Potential toxicity of polystyrene microplastic particles. Sci Rep 10, 7391. https://doi.org/10.1038/s41598-020-64464-9

Inkielewicz-Stepniak, I., Tajber, L., Behan, G., Zhang, H., Radomski, M.W., Medina, C., Santos-Martinez, M.J., 2018. The Role of Mucin in the Toxicological Impact of Polystyrene Nanoparticles. Materials 11, 724. https://doi.org/10.3390/ma11050724

Jiang, B., Kauffman, A.E., Li, L., McFee, W., Cai, B., Weinstein, J., Lead, J.R., Chatterjee, S., Scott, G.I., Xiao, S., 2020. Health impacts of environmental contamination of micro- and nanoplastics: a review. Environ Health Prev Med 25, 29. https://doi.org/10.1186/s12199-020-00870-9

Jin, Y., Lu, L., Tu, W., Luo, T., Fu, Z., 2019. Impacts of polystyrene microplastic on the gut barrier, microbiota and metabolism of mice. Science of The Total Environment 649, 308–317. https://doi.org/10.1016/j.scitotenv.2018.08.353

Kannan, K., Vimalkumar, K., 2021. A Review of Human Exposure to Microplastics and Insights Into Microplastics as Obesogens. Front Endocrinol (Lausanne) 12, 724989. https://doi.org/10.3389/fendo.2021.724989

Koblitz J., Dirks, W.G., Eberth, S., Nagel, S., Steenpass, L., Pommerenke, C., 2022. ACC-313 | Cell lines | DSMZCellDive [WWW Document]. DSMZCellDive. URL https://celldive.dsmz.de/cellline/ACC-313 (accessed 2.7.23).

Kulkarni, S.A., Feng, S.-S., 2013. Effects of Particle Size and Surface Modification on Cellular Uptake and Biodistribution of Polymeric Nanoparticles for Drug Delivery. Pharm Res 30, 2512–2522. https://doi.org/10.1007/s11095-012-0958-3

Kumari, S., Mg, S., Mayor, S., 2010. Endocytosis unplugged: multiple ways to enter the cell. Cell Res 20, 256–275. https://doi.org/10.1038/cr.2010.19

Landrigan, P.J., Stegeman, J.J., Fleming, L.E., Allemand, D., Anderson, D.M., Backer, L.C., Brucker-Davis, F., Chevalier, N., Corra, L., Czerucka, D., Bottein, M.-Y.D., Demeneix, B., Depledge, M., Deheyn, D.D., Dorman, C.J., Fénichel, P., Fisher, S., Gaill, F., Galgani, F., Gaze, W.H., Giuliano, L., Grandjean, P., Hahn, M.E., Hamdoun, A., Hess, P., Judson, B., Laborde, A., McGlade, J., Mu, J., Mustapha, A., Neira, M., Noble, R.T., Pedrotti, M.L., Reddy, C., Rocklöv, J., Scharler, U.M., Shanmugam, H., Taghian, G., van de Water, J.A.J.M., Vezzulli, L., Weihe, P., Zeka, A., Raps, H., Rampal, P., n.d. Human Health and Ocean Pollution. Ann Glob Health 86, 151. https://doi.org/10.5334/aogh.2831

Li, B., Ding, Y., Cheng, X., Sheng, D., Xu, Z., Rong, Q., Wu, Y., Zhao, H., Ji, X., Zhang, Y., 2020. Polyethylene microplastics affect the distribution of gut microbiota and inflammation development in mice. Chemosphere 244, 125492. https://doi.org/10.1016/j.chemosphere.2019.125492

Lithner, D., Larsson, Å., Dave, G., 2011. Environmental and health hazard ranking and assessment of plastic polymers based on chemical composition. Science of The Total Environment 409, 3309–3324. https://doi.org/10.1016/j.scitotenv.2011.04.038

Liu, L., Xu, K., Zhang, B., Ye, Y., Zhang, Q., Jiang, W., 2021. Cellular internalization and release of polystyrene microplastics and nanoplastics. Science of The Total Environment 779, 146523. https://doi.org/10.1016/j.scitotenv.2021.146523

Liu, P., Qian, L., Wang, H., Zhan, X., Lu, K., Gu, C., Gao, S., 2019. New Insights into the Aging Behavior of Microplastics Accelerated by Advanced Oxidation Processes. Environ. Sci. Technol. 53, 3579–3588. https://doi.org/10.1021/acs.est.9b00493

Llorca, M., Farré, M., 2021. Current Insights into Potential Effects of Micro-Nanoplastics on Human Health by in-vitro Tests. Frontiers in Toxicology 3.

Manzanares, D., Ceña, V., 2020. Endocytosis: The Nanoparticle and Submicron Nanocompounds Gateway into the Cell. Pharmaceutics 12, 371. https://doi.org/10.3390/pharmaceutics12040371

Martínez-Maqueda, D., Miralles, B., Recio, I., 2015. HT29 Cell Line, The Impact of Food Bioactives on Health: in vitro and ex vivo models [Internet]. Springer. https://doi.org/10.1007/978-3-319-16104-4_11

Mehta, D., Malik, A.B., 2006. Signaling Mechanisms Regulating Endothelial Permeability. Physiological Reviews 86, 279–367. https://doi.org/10.1152/physrev.00012.2005

MSKCC, n.d. HT-29: Human Colorectal Adenocarcinoma Cell Line (ATCC HTB-38) | Memorial Sloan Kettering Cancer Center [WWW Document]. URL https://www.mskcc.org/research-advantage/support/technology/tangible-material/human-colorectal-adenocarcinoma-cell-line-ht-29 (accessed 2.6.23).

Paddock, S.W., 2000. Principles and Practices of Laser Scanning Confocal Microscopy. MB 16, 127–150. https://doi.org/10.1385/MB:16:2:127
Patel, D., Mamtora, D., Kamath, A., Shukla, A., 2022. Rogue one: A plastic story. Marine Pollution Bulletin 177, 113509. https://doi.org/10.1016/j.marpolbul.2022.113509
Paul, M.B., Stock, V., Cara-Carmona, J., Lisicki, E., Shopova, S., Fessard, V., Braeuning, A., Sieg, H., Böhmert, L., n.d. Micro- and nanoplastics – current state of knowledge with the focus on oral uptake and toxicity. Nanoscale Adv 2, 4350–4367. https://doi.org/10.1039/d0na00539h
PlasticsEurope, 2022. Plastics - the Facts 2022 • Plastics Europe. Plastics Europe. URL https://plasticseurope.org/knowledge-hub/plastics-the-facts-2022/ (accessed 11.12.22).
PlasticsEurope, 2019. Plastics - the Facts 2019. Plastics Europe DE. URL https://plasticseurope.org/de/knowledge-hub/plastics-the-facts-2019-2/ (accessed 11.9.22).
PlasticsEurope, 2018. Plastics - the Facts 2018 • Plastics Europe. Plastics Europe. URL https://plasticseurope.org/knowledge-hub/plastics-the-facts-2018/ (accessed 11.18.22).
PlasticsEurope, 2012. PlasticsTheFacts_2012_EN_FINAL-screen_Plastics The Facts EN 40.
Prata, J.C., da Costa, J.P., Lopes, I., Duarte, A.C., Rocha-Santos, T., 2020. Environmental exposure to microplastics: An overview on possible human health effects. Science of The Total Environment 702, 134455. https://doi.org/10.1016/j.scitotenv.2019.134455
Rennick, J.J., Johnston, A.P.R., Parton, R.G., 2021. Key principles and methods for studying the endocytosis of biological and nanoparticle therapeutics. Nat. Nanotechnol. 16, 266–276. https://doi.org/10.1038/s41565-021-00858-8
Revel, M., Châtel, A., Mouneyrac, C., 2018. Micro(nano)plastics: A threat to human health? Current Opinion in Environmental Science & Health, Micro and Nanoplastics Edited by Dr. Teresa A.P. Rocha-Santos 1, 17–23. https://doi.org/10.1016/j.coesh.2017.10.003
Rowenczyk, L., Dazzi, A., Deniset-Besseau, A., Beltran, V., Goudounèche, D., Wong-Wah-Chung, P., Boyron, O., George, M., Fabre, P., Roux, C., Mingotaud, A.-F., ter Halle, A., 2020. Microstructure Characterization of Oceanic Polyethylene Debris. Environmental Science and Technology 54, 4102–4109. https://doi.org/10.1021/acs.est.9b07061
Rubio, L., Marcos, R., Hernández, A., 2020. Potential adverse health effects of ingested micro- and nanoplastics on humans. Lessons learned from in vivo and in vitro mammalian models. Journal of Toxicology and Environmental Health, Part B 23, 51–68. https://doi.org/10.1080/10937404.2019.1700598
Rudolph, J., Völkl, M., Jérôme, V., Scheibel, T., Freitag, R., 2021. Noxic effects of polystyrene microparticles on murine macrophages and epithelial cells. Sci Rep 11, 15702. https://doi.org/10.1038/s41598-021-95073-9
Schneeberger, E.E., Lynch, R.D., 2004. The tight junction: a multifunctional complex. American Journal of Physiology-Cell Physiology 286, C1213–C1228. https://doi.org/10.1152/ajpcell.00558.2003
Schwabl, P., Köppel, S., Königshofer, P., Bucsics, T., Trauner, M., Reiberger, T., Liebmann, B., 2019. Detection of Various Microplastics in Human Stool. Ann Intern Med 171, 453–457. https://doi.org/10.7326/M19-0618
Sendra, M., Pereiro, P., Figueras, A., Novoa, B., 2021. An integrative toxicogenomic analysis of plastic additives. Journal of Hazardous Materials 409, 124975. https://doi.org/10.1016/j.jhazmat.2020.124975
Seydoux, E., Rothen-Rutishauser, B., Nita, I., Balog, S., Gazdhar, A., Stumbles, P., Fink, A., Blank, F., Von Garnier, C., 2014. Size-dependent accumulation of particles in lysosomes modulates dendritic cell function through impaired antigen degradation. International journal of nanomedicine 9, 3885–902. https://doi.org/10.2147/IJN.S64353
Shang, L., Nienhaus, K., Nienhaus, G.U., 2014. Engineered nanoparticles interacting with cells: size matters. J Nanobiotechnology 12, 5. https://doi.org/10.1186/1477-3155-12-5
Shi, X., Wang, X., Huang, R., Tang, C., Hu, C., Ning, P., Wang, F., 2022. Cytotoxicity and Genotoxicity of Polystyrene Micro- and Nanoplastics with Different Size and Surface Modification in A549 Cells. Int J Nanomedicine 17, 4509–4523. https://doi.org/10.2147/IJN.S381776

Stock, V., Böhmert, L., Lisicki, E., Block, R., Cara-Carmona, J., Pack, L.K., Selb, R., Lichtenstein, D., Voss, L., Henderson, C.J., Zabinsky, E., Sieg, H., Braeuning, A., Lampen, A., 2019. Uptake and effects of orally ingested polystyrene microplastic particles in vitro and in vivo. Arch Toxicol 93, 1817–1833. https://doi.org/10.1007/s00204-019-02478-7

Visalli, G., Facciolà, A., Pruiti Ciarello, M., De Marco, G., Maisano, M., Di Pietro, A., 2021. Acute and Sub-Chronic Effects of Microplastics (3 and 10 μm) on the Human Intestinal Cells HT-29. International Journal of Environmental Research and Public Health 18, 5833. https://doi.org/10.3390/ijerph18115833

Wang, F., Bexiga, M.G., Anguissola, S., Boya, P., Simpson, J.C., Salvati, A., Dawson, K.A., 2013. Time resolved study of cell death mechanisms induced by amine-modified polystyrene nanoparticles. Nanoscale 5, 10868. https://doi.org/10.1039/c3nr03249c

Whetzel PL, Noy NF, Shah NH, Alexander PR, Nyulas C, Tudorache T, Musen MA, 2011. BRENDA Tissue and Enzyme Source Ontology - SW-480 cell - Classes | NCBO BioPortal [WWW Document]. NCBO BioPortal. URL https://bioportal.bioontology.org/ontologies/BTO?p=classes&conceptid=http%3A%2F%2Fpurl.obolibrary.org%2Fobo%2FBTO_0000038 (accessed 2.7.23).

Wilcox, C., Mallos, N.J., Leonard, G.H., Rodriguez, A., Hardesty, B.D., 2016. Using expert elicitation to estimate the impacts of plastic pollution on marine wildlife. Marine Policy 65, 107–114. https://doi.org/10.1016/j.marpol.2015.10.014

Wu, B., Wu, X., Liu, S., Wang, Z., Chen, L., 2019. Size-dependent effects of polystyrene microplastics on cytotoxicity and efflux pump inhibition in human Caco-2 cells. Chemosphere 221, 333–341. https://doi.org/10.1016/j.chemosphere.2019.01.056

Yong, C.Q.Y., Valiyaveettil, S., Tang, B.L., 2020. Toxicity of Microplastics and Nanoplastics in Mammalian Systems. Int J Environ Res Public Health 17, 1509. https://doi.org/10.3390/ijerph17051509

Zhang, N., Li, Y.B., He, H.R., Zhang, J.F., Ma, G.S., 2021. You are what you eat: Microplastics in the feces of young men living in Beijing. Science of The Total Environment 767, 144345. https://doi.org/10.1016/j.scitotenv.2020.144345

8. Appendices

Appendix A

Size-dependent uptake of PS-MNP particles

A1. HT29

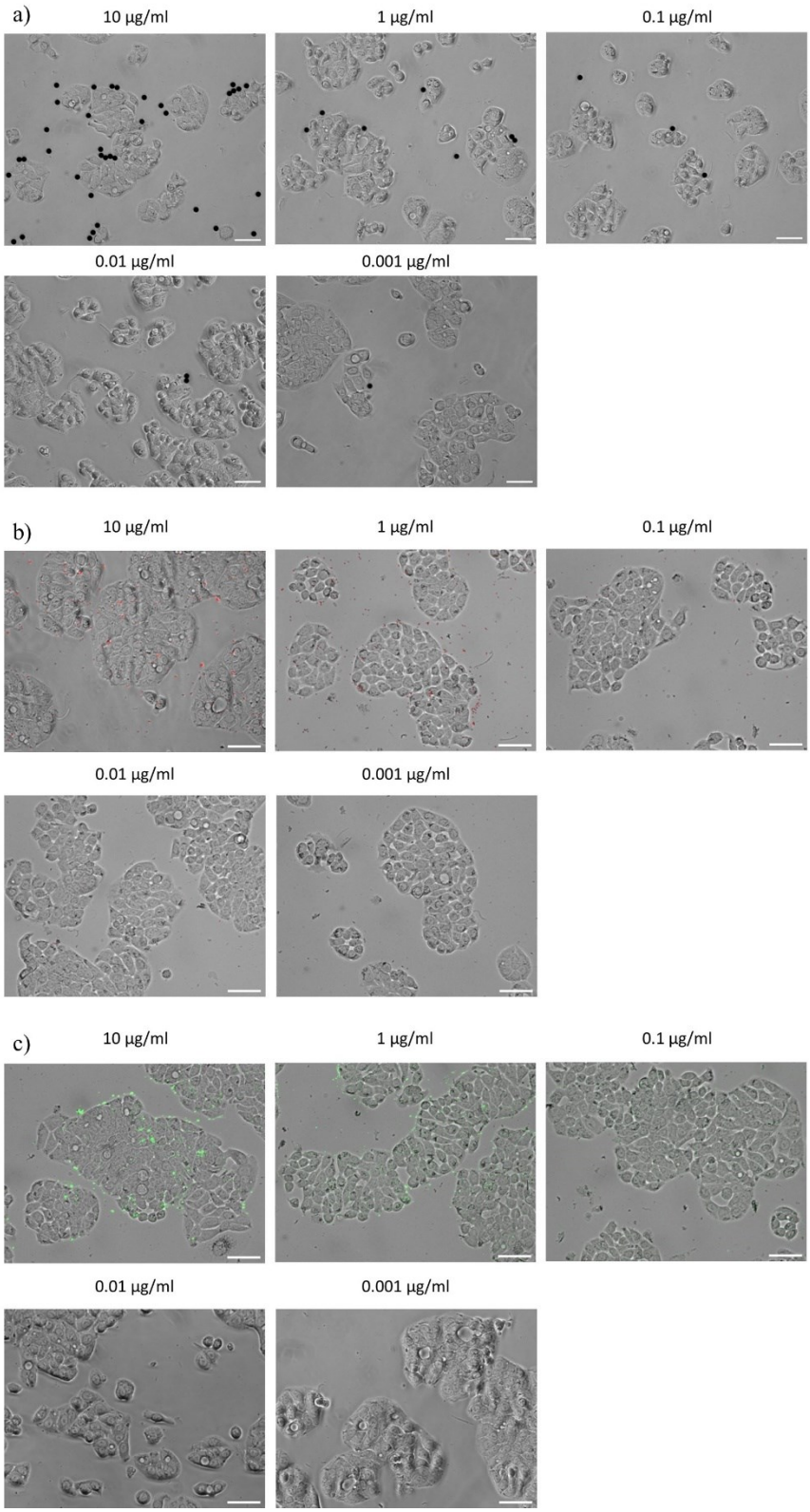

Figure A17. Fluorescence microscope images of HT29 cells. Cells were exposed to five different

concentrations of PS 9.55, 1.14 and 0.235 µm particles for 24 hours. Brightfield images of blue coloured 9.55 µm particles (a), multichannel fluorescence images of red fluorescent 1.14 µm (b), and green fluorescent 0.235 µm (c) PS particles. For the red and green fluorescence the filter blocks TRITC (EX 540/26, DM 565, EM 605/56) and FITC (EM 480/15, DM 505, EM 535/40) were used, respectively. Scale bar: 50 µm.

Both the 9.55, 1.14 and 0.235 µm PS particles showed an uneven (heterogeneous) distribution in the wells. It was observed that some cells had absorbed more nanoparticles than neighbouring cells and that in some cells more particles had accumulated around or on the cells. Furthermore, it must be considered that with this set up, not only diffusion but also sedimentation contributes to particle uptake. Accordingly, the actual concentration of particles on the cell surface and number of particles taken up by the cells may be higher and thus differ from the initial value (the initial mass concentration).

A2. HCT116

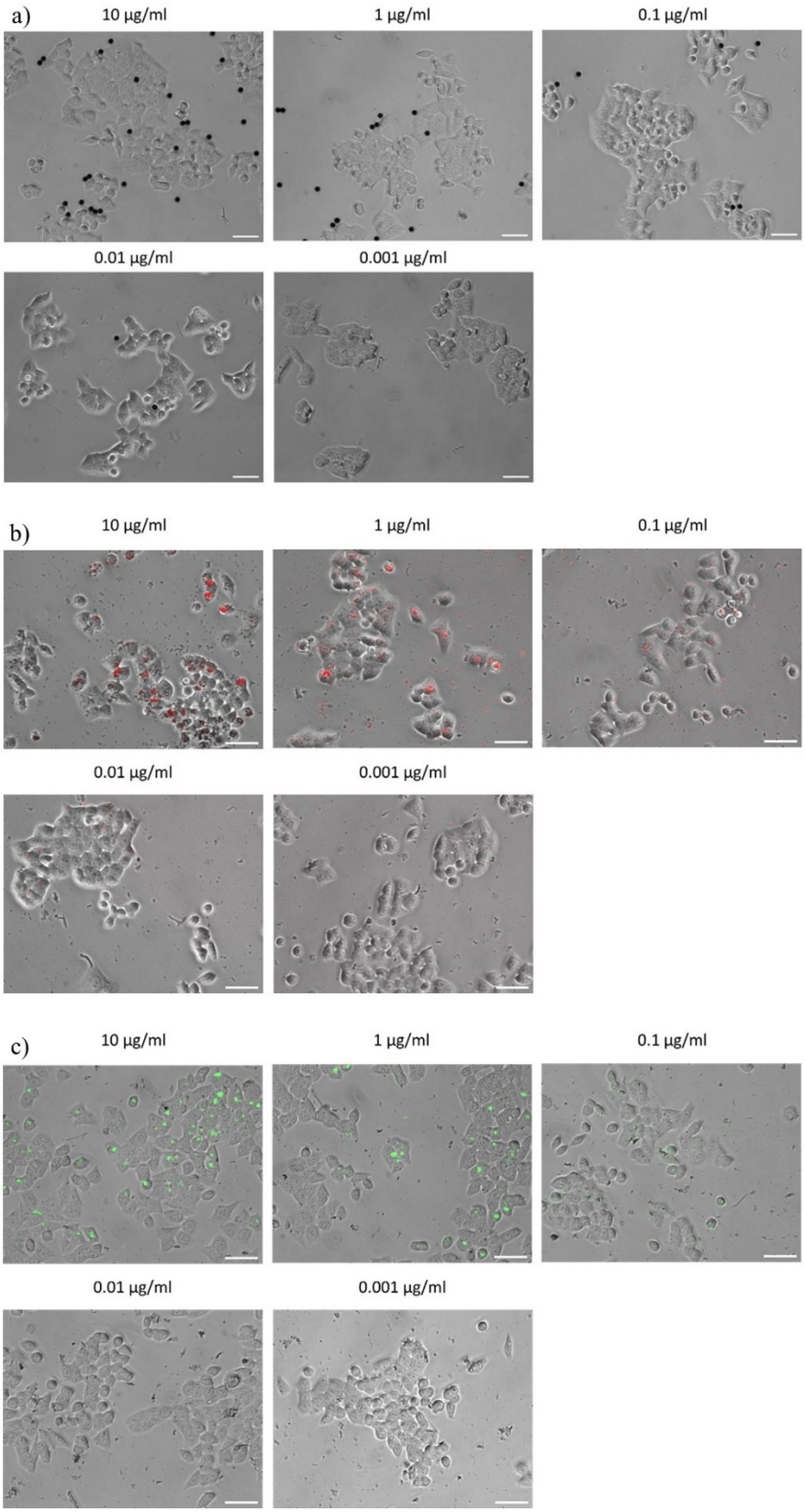

Figure A18. Fluorescence microscope images of HCT116 cells. Cells were exposed to five different concentrations of PS 9.55, 1.14 and 0.235 µm particles for 24 hours. Brightfield images of blue

coloured 9.55 µm particles (a), multichannel fluorescence images of red fluorescent 1.14 µm (b) (TRITC filter; EX 540/26, DM 565, EM 605/56) and green fluorescent 0.235 µm (c) PS particles (FITC filter; EM 480/15, DM 505, EM 535/40). Scale bar: 50 µm.

A3. SW480

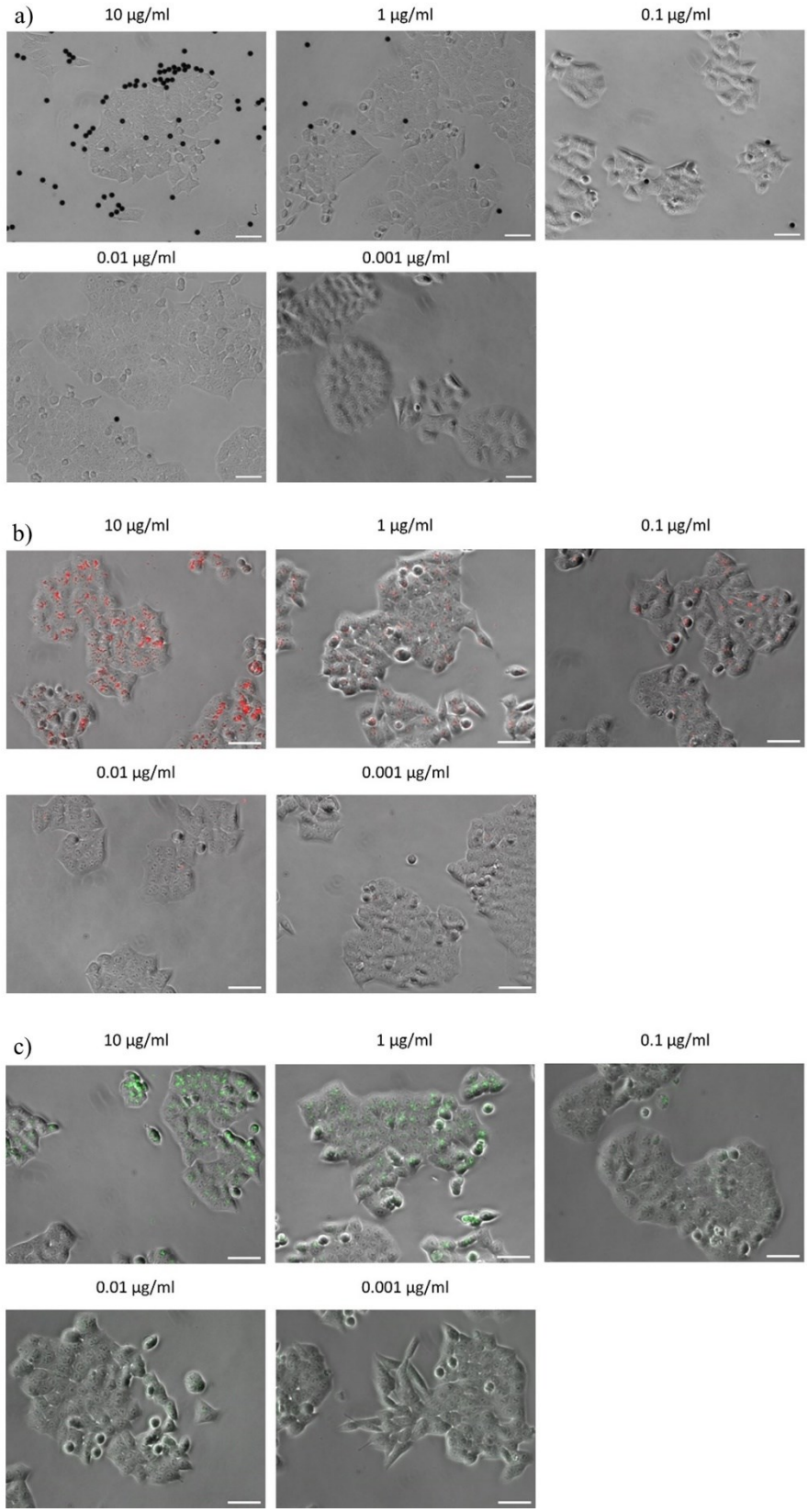

Figure A19. Fluorescence microscope images of SW480 cells. Treatment for 24 hours with five different concentrations of 9.55, 1.14 and 0.235 µm PS particles. Brightfield images of blue coloured

9.55 µm particles (a), multichannel fluorescence images of red fluorescent 1.14 µm (b) (TRITC filter; EX 540/26, DM 565, EM 605/56) and green fluorescent 0.235 µm (c) PS particles (FITC filter; EM 480/15, DM 505, EM 535/40). Scale bar: 50 µm.

A4. SW620

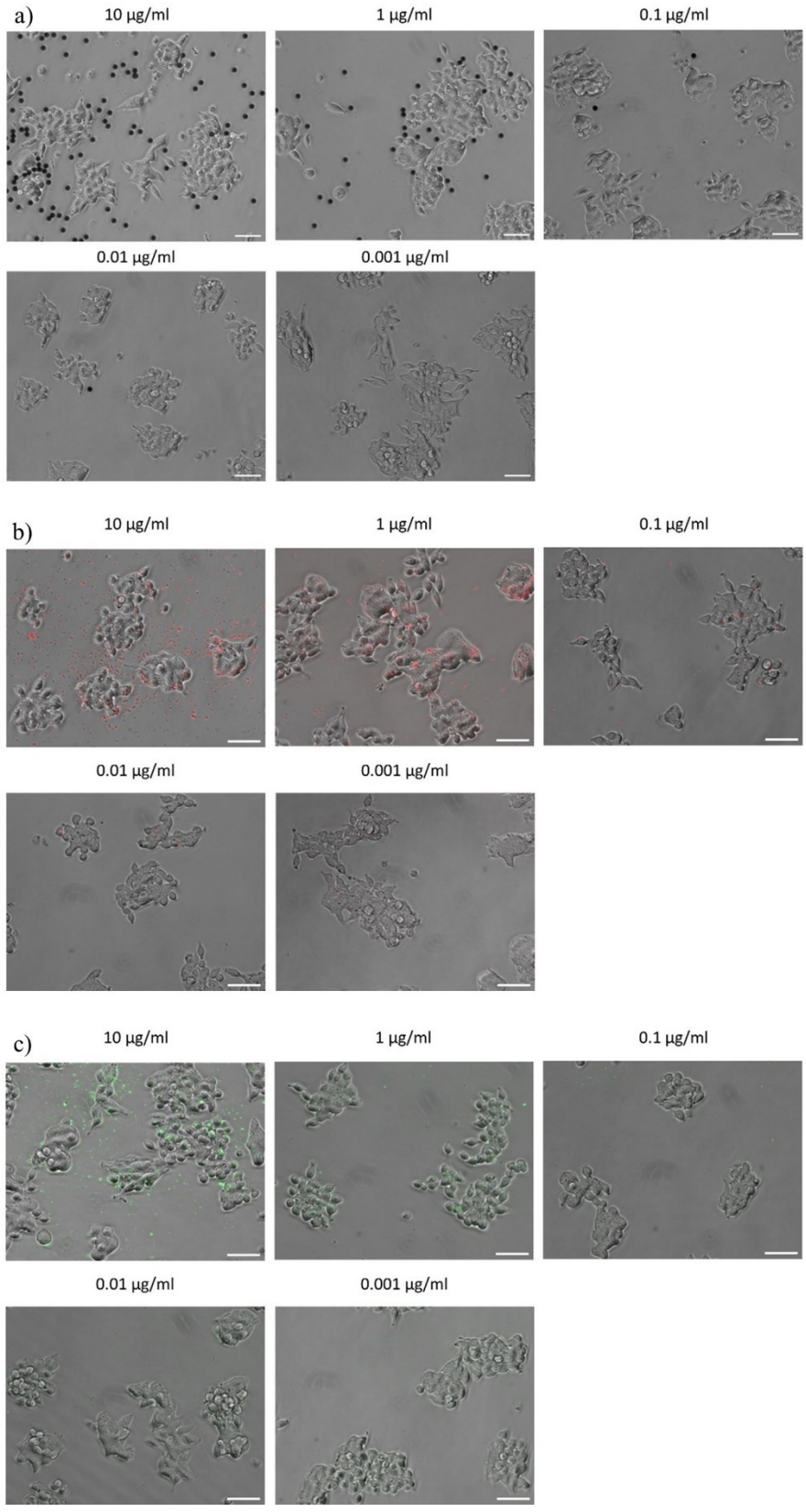

Figure A20. Fluorescence microscope images of SW620 cells. Treatment for 24 hours with five different concentrations of 9.55, 1.14 and 0.235 µm PS particles. Brightfield images of blue coloured

9.55 µm particles (a), multichannel fluorescence images of red fluorescent 1.14 µm (b) (TRITC filter; EX 540/26, DM 565, EM 605/56) , and green fluorescent 0.235 µm (c) PS particles (FITC filter; EM 480/15, DM 505, EM 535/40). Scale bar: 50 µm.

Appendix B

Detection of 1.14 and 0.235 µm spherical PS particle

B1. Measurements of 1.14 µm PS particles as double positive signals

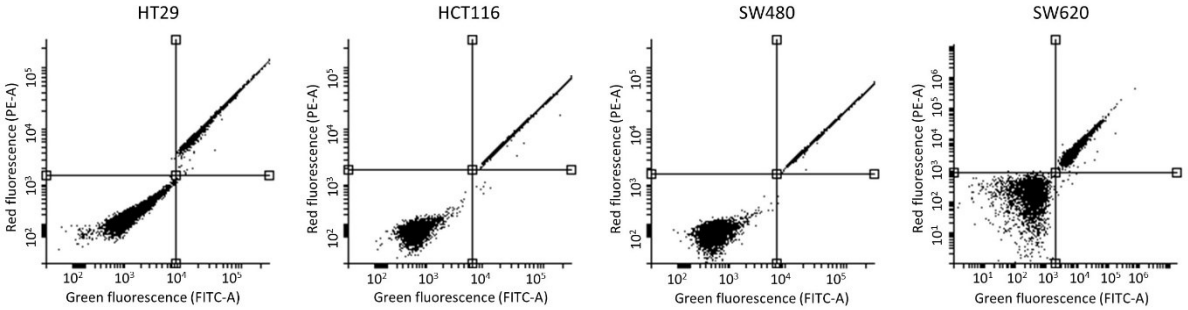

Figure B1. Dot plots depicting the fluorescence signal of 1.14 µm PS particle. Cells were treated for 24 hours with 1 µg/ml of 1.14 µm PS particles. The 1.14 µm particles were measured as double positive signals, since they showed fluorescent activity not only in the red (PE) but also in the green channel (FITC) (population on the right top). The population on the left bottom corresponds to the cells that have not taken up any particles. The upper right quadrant constitute the population of cells that have internalized particles.

B2. Measurements of 0.235 µm PS particles in the green channel (FITC-A)

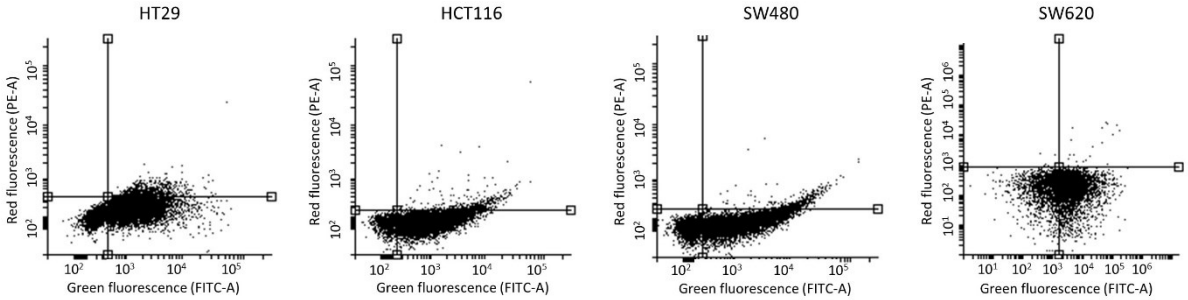

Figure B2. Dot plots depicting the fluorescence signal of 0.235 µm PS particle. Cells were treated for 24 hours with 1 µg/ml of 0.235 µm PS particles. The 0.235 µm particles are only fluorescently active in the green channel (FITC) (population on the right bottom). The population on the left bottom corresponds to the cells that have not taken up any particles. The lower right quadrant constitute the population of cells that have internalized particles. Since the fluorescence of the particles is additive, the intensity of intracellular fluorescence indicates the amount of internalized particles. Increasing fluorescence values in the green channel thus indicate that more particles have been taken up per cell.

Appendix C

Intake assessment by flow cytometry

C1. Particle counting

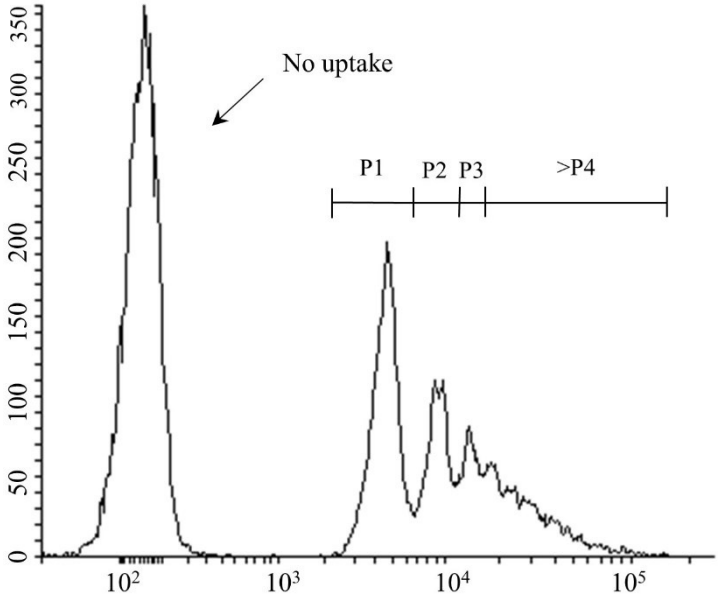

Figure C1. Representative histogram of the fluorescence distribution of HCT116 cells after 24 h incubation with red fluorescent 1.14 µm PS particles. The separate peaks of the histogram correspond respectively to the number of internalized 1.14 µm PS particles per cell. The first peak on the left consist of cells that did not adsorb any particles. The second to fourth peak (P1-P3) is correlated to cells that have taken up one, two or three particles, respectively. The fifth peak (>P4) corresponds to cells that have internalized four or more particles.

C2. Particle – cell interactions at different concentrations

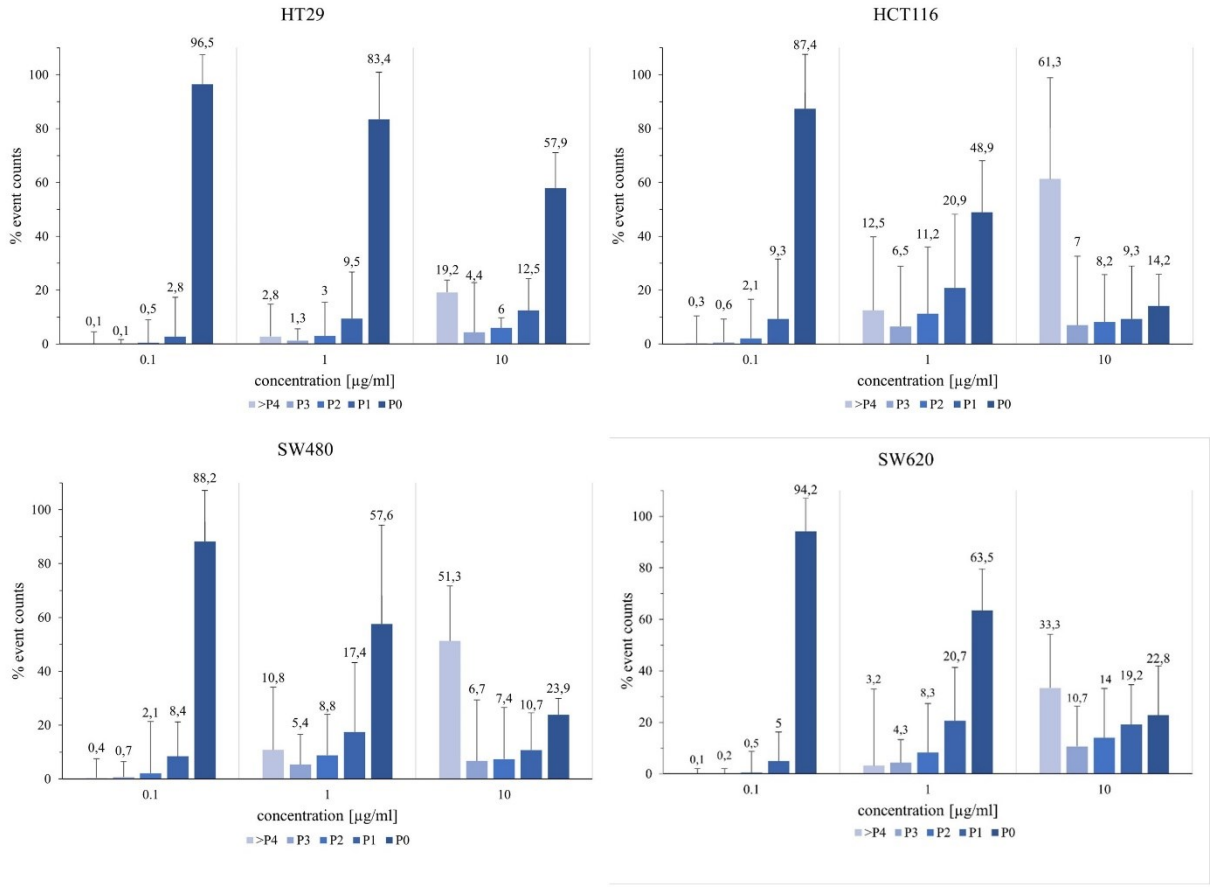

Figure C2. Identification of cell populations with different numbers of internalized 1.14 µm PS particles at 3 different concentrations. Values given in the bar graphs show the percentage of particle-positive cells.